J. Fluid Mech. (1995), *vol.* 288, *pp.* 351–381

Modified Boussinesq equations and associated parabolic models for water wave propagation

By YONGZE CHEN† AND PHILIP L.-F. LIU

School of Civil and Environmental Engineering, Cornell University, Ithaca, NY 14853, USA

(Received 12 April 1994 and in revised form 8 November 1994)

The modified Boussinesq equations given by Nwogu (1993*a*) are rederived in terms of a velocity potential on an arbitrary elevation and the free surface displacement. The optimal elevation where the velocity potential should be evaluated is determined by comparing the dispersion and shoaling properties of the linearized modified Boussinesq equations with those given by the linear Stokes theory over a range of depths from zero to one half of the equivalent deep-water wavelength. For regular waves consisting of a finite number of harmonics and propagating over a slowly varying topography, the governing equations for velocity potentials of each harmonic are a set of weakly nonlinear coupled fourth-order elliptic equations with variable coefficients. The parabolic approximation is applied to these coupled fourth-order elliptic equations for the first time. A small-angle parabolic model is developed for waves propagating primarily in a dominant direction. The pseudospectral Fourier method is employed to derive an angular-spectrum parabolic model for multi-directional wave propagation. The small-angle model is examined by comparing numerical results with Whalin's (1971) experimental data. The angular-spectrum model is tested by comparing numerical results with the refraction theory of cnoidal waves (Skovgaard & Petersen 1977) and is used to study the effect of the directed wave angle on the oblique interaction of two identical cnoidal wavetrains in shallow water.

1. Introduction

Boussinesq-type equations have been commonly used to describe weakly nonlinear and weakly dispersive wave propagation in shallow water. These equations are derived based on the assumption that the weak nonlinearity represented by the ratio of wave amplitude to water depth, $\epsilon = a_0/h_0$, is in the same order of magnitude as the frequency dispersion denoted by the square of the ratio of water depth to wavelength, $\mu^2 = (h_0/l_0)^2$.

A major limitation of Boussinesq-type equations is that they are only applicable to a relatively shallow water depth. For example, to keep errors of the phase velocity estimated by the best form of the linearized Boussinesq equations within 5% of that determined from the linear Stokes theory, the water depth has to be less than about one-fifth of the equivalent deep-water wavelength (Madsen, Murray & Sørensen 1991). For short waves or in intermediate depths, Boussinesq-type equations are incapable of describing wave propagation correctly, or even worse, they may become unstable. This behaviour poses two difficulties in modelling water wave propagation.

† Present address: Center For Coastal Studies, Scripps Institution of Oceanography, University of California, San Diego, La Jolla, CA 92093-0209, USA.

Firstly, one has to use different equations in different water depths and deal with the difficulty of matching these equations. Secondly, even in the shallow-water region numerically generated short waves will produce erroneous results and could cause instabilities.

Recently, numerous attempts have been made to extend the range of applicability of Boussinesq-type equations to deep water by improving their linear dispersion characteristics. Witting (1984) used a set of conservative equations to investigate wave propagation in a constant-depth channel bounded by two rigid impermeable walls. The depth-averaged and mean free surface velocities used in his Boussinesq-type equations were expanded into a Taylor series in terms of a pseudo-velocity. Coefficients in the series were then determined to yield a Padé approximation to the Taylor expansion of the dispersion relation given by the linear Stokes wave theory. Using the [2/2] Padé approximation, Witting obtained good results for both short and long waves. However, it is difficult to extend Witting's approach to two horizontal dimensions with a varying depth.

McCowan & Blackman (1989) modified the conventional Boussinesq equations (Peregrine 1967) by introducing an effective depth and a dispersion tuning parameter, which were chosen to match the dispersion properties of the first-order Stokes waves. In shallow water the effective depth is identical to the actual depth, whereas in deeper water the effective depth is restricted to the upper part of the water where most of the wave action occurs. Such an approach is, however, only applicable to monochromatic waves and it is not clear if it is applicable to a varying topography.

Madsen *et al.* (1991) formulated the conventional Boussinesq equations for constant depth in terms of volume flux components instead of the depth-averaged velocity components. They included in the momentum equations some higher-order terms, which were conventionally neglected in the process of deriving the Boussinesq equations, and obtained a new form of Boussinesq equations. The weighting factor for these higher-order terms is adjusted so that the linear dispersion characteristics of the resulting Boussinesq-type equations are remarkably improved. Madsen & Sørensen (1992) extended this set of Boussinesq-type equations for a slowly varying topography and introduced the linear shoaling gradient as another quantity to measure the improvement of the new equations.

Nwogu (1993*a*) formally derived an alternative form of the Boussinesq equations in terms of a horizontal velocity on an arbitrary elevation. He showed that from intermediate depth to deep water, the linear dispersion characteristics of the new set of equations are strongly dependent on the choice of the velocity variable. The linear dispersion properties become very similar to those of the first-order Stokes waves if a velocity close to mid-depth is selected as the velocity variable. This makes the new set of equations applicable to regular and irregular waves travelling from relatively deep water to shallow water. The highest order of the spatial derivatives in the equations derived by Nwogu is one order higher than that in the conventional Boussinesq equations. This creates a difficulty in specifying appropriate boundary conditions and increases the numerical effort for solving these new equations.

On the other hand, the parabolic approximation has been developed rapidly as an efficient and practical tool for modelling wave propagation over large coastal areas. The parabolic approximation, typically involving converting an elliptic equation into a parabolic equation, not only reduces the computational efforts dramatically but also alleviates the burden of imposing the down-wave boundary conditions, which usually are unknown *a priori* for most coastal hydrodynamic problems. For regu-

lar waves consisting of a finite number of harmonics, Liu, Yoon & Kirby (1985) developed the first parabolic approximation model for the conventional Boussinesq equations. In their model waves must propagate in a dominant direction. Therefore, it is a small-angle parabolic approximation model. Recently, Kirby (1990) used the discrete angular spectrum method to develop a parabolic model for the conventional Boussinesq equations, in which the topography is allowed to vary only in the on-offshore direction. The parabolic approximation cannot be directly applied to Nwogu's new Boussinesq-type equations, in which the horizontal velocity components and the free surface displacement are coupled together. The reason is that in the process of combining the governing equations into one equation in terms of the free surface displacement, the improvement made in dispersion properties cannot be preserved.

The primary objective of this paper is to develop parabolic approximation models based on the modified Boussinesq equations. We first rederive Nwogu's modified Boussinesq equations in terms of a velocity potential on an arbitrary elevation and the free surface displacement. The optimal elevation for the velocity potential is determined by comparing the dispersion and shoaling properties of the linearized modified Boussinesq equations with those given by the linear Stokes theory over a range of water depths from zero to one half of the equivalent deep-water wavelength. Because the governing equations can be combined into one equation in terms of the velocity potential while the improved linear dispersion properties are still preserved, we are able to apply the parabolic approximation. For regular waves propagating over a slowly varying topography, the governing equations for velocity potentials of each harmonic are a set of weakly nonlinear coupled fourth-order elliptic equations with variable coefficients. Up to now, all the existing parabolic models in water wave dynamics are based on second-order elliptic equations, such as the mild-slope equation. As far as we know, no one has applied the parabolic approximation to a non-homogeneous fourth-order ordinary or partial differential equation. In this paper we present a new approach to develop the parabolic approximation to a variable-coefficient fourth-order 'ordinary' differential equation with weak forcing, which may involve the other independent variable (see (4.14)). We find out that the accuracy of the parabolic approximation depends on the difference between the wavenumber of the forcing term and the characteristic wavenumber of the equation (i.e. the real root of the dispersion relation for the corresponding homogenous equation). For waves propagating primarily in a dominant direction, the governing equation for each harmonic can be rewritten formally as a fourth-order 'ordinary' differential equation with weak forcing depending on both independent variables. A small-angle parabolic model is developed and the justification of this model is discussed. The pseudospectral Fourier method used by Chen & Liu (1994) is extended to derive an angular-spectrum parabolic model for multi-directional wave propagation: the wave field is first decomposed into a series of wave modes by the pseudospectral Fourier method; then, the parabolic approximation is used to approximate the governing equations for each wave mode, which are a set of weakly coupled fourth-order ordinary differential equations. The small-angle model is tested by comparing numerical results with experimental data (Whalin 1971). The angular-spectrum model is examined by comparing the model results with the refraction theory of cnoidal waves (Skovgaard & Petersen 1977) and then is used to study the effect of the directed wave angle on the oblique interaction of two identical cnoidal waves. Finally, in concluding remarks we present an empirical formula to calculate the velocity wave field in relatively deep water.

2. Modified Boussinesq equations

Consider a wave field bounded by a free surface $z' = \zeta'(x', y', t')$ and a stationary bottom $z' = -h'(x', y')$. A Cartesian coordinate system is adopted, with the x'-axis and the y'-axis locating on the still water plane and the z'-axis pointing vertically upwards. Let h_0, l_0 and a_0 denote the characteristic water depth, wavelength and wave amplitude, respectively. The following dimensionless variables are defined:

$$\left.\begin{aligned} x &= \frac{x'}{l_0}, \quad y = \frac{y'}{l_0}, \quad z = \frac{z'}{h_0}, \quad t = \frac{c_0}{l_0}t', \\ \zeta &= \frac{\zeta'}{a_0}, \qquad h = \frac{h'}{h_0}, \qquad \Phi = \frac{h_0}{a_0 l_0 c_0}\Phi', \end{aligned}\right\} \tag{2.1}$$

where $c_0 = (gh_0)^{1/2}$ is the linear-long-wave speed and Φ is the velocity potential; primes are used for dimensional variables.

The dimensionless governing equations and boundary conditions for a potential flow with a free surface are

$$\mu^2 \nabla^2 \Phi + \frac{\partial^2 \Phi}{\partial z^2} = 0, \qquad -h < z < \epsilon\zeta, \tag{2.2}$$

$$\frac{\partial \Phi}{\partial z} = \mu^2 \left(\frac{\partial \zeta}{\partial t} + \epsilon \nabla \Phi \cdot \nabla \zeta \right) \quad \text{on} \quad z = \epsilon\zeta, \tag{2.3}$$

$$\frac{\partial \Phi}{\partial z} = -\mu^2 \nabla \Phi \cdot \nabla h \quad \text{on} \quad z = -h, \tag{2.4}$$

$$\left(\frac{\partial \Phi}{\partial t} + \zeta \right) + \frac{\epsilon}{2} \left[(\nabla \Phi)^2 + \frac{1}{\mu^2} \left(\frac{\partial \Phi}{\partial z} \right)^2 \right] = 0 \quad \text{on} \quad z = \epsilon\zeta, \tag{2.5}$$

where $\epsilon = a_0/h_0$ and $\mu^2 = (h_0/l_0)^2$ are parameters measuring nonlinearity and frequency dispersion, respectively, and $\nabla = (\partial_x, \partial_y)$. We assume that $O(\epsilon) = O(\mu^2) \ll 1$.

Integrating (2.2) from $z = -h$ to $z = \epsilon\zeta$ and applying the kinematic boundary conditions (2.3) and (2.4), we obtain

$$\nabla \cdot \left[\int_{-h}^{\epsilon\zeta} \nabla \Phi \, dz \right] + \frac{\partial \zeta}{\partial t} = 0. \tag{2.6}$$

Expanding the velocity potential Φ as

$$\Phi = \sum_{n=0}^{\infty} \mu^{2n} \Phi_n(x, y, z, t) \tag{2.7}$$

and substituting (2.7) into (2.2) and (2.4), we collect terms with multiplies of like order of even powers of μ:

$$\left.\begin{aligned} &\frac{\partial^2 \Phi_0}{\partial z^2} = 0, \qquad -h < z < \epsilon\zeta, \quad \frac{\partial \Phi_0}{\partial z} = 0 \qquad \text{on} \quad z = -h; \\ &\frac{\partial^2 \Phi_1}{\partial z^2} = -\nabla^2 \Phi_0, \quad -h < z < \epsilon\zeta, \quad \frac{\partial \Phi_1}{\partial z} = -\nabla \Phi_0 \cdot \nabla h \quad \text{on} \quad z = -h; \\ &\vdots \end{aligned}\right\} \tag{2.8}$$

The general solution to Φ_n $(n = 0, 1, \ldots)$ in (2.8) can be expressed as

$$\left.\begin{aligned} \Phi_0 &= \phi_{00}(x, y, t), \\ \Phi_1 &= \phi_{10}(x, y, t) - z\nabla \cdot (h\nabla\phi_{00}) - \tfrac{1}{2}z^2\nabla^2\phi_{00}, \\ &\vdots \end{aligned}\right\} \tag{2.9}$$

where $\phi_{00}(x, y, t)$, $\phi_{10}(x, y, t)$, etc. are constants of integration with respect to z. Hence, expansion (2.7) can be rewritten as

$$\Phi(x, y, z, t) = \phi_{00} + \mu^2\left[\phi_{10} - z\nabla \cdot (h\nabla\phi_{00}) - \frac{z^2}{2}\nabla^2\phi_{00}\right] + O(\mu^4). \tag{2.10}$$

Denoting $\Phi_\alpha(x, y, t)$ as the velocity potential on an arbitrary elevation $z = z_\alpha(x, y)$, from (2.10) we obtain

$$\begin{aligned} \Phi_\alpha(x, y, t) &= \Phi(x, y, z_\alpha(x, y), t) \\ &= \phi_{00} + \mu^2\left[\phi_{10} - z_\alpha\nabla \cdot (h\nabla\phi_{00}) - \frac{z_\alpha^2}{2}\nabla^2\phi_{00}\right] + O(\mu^4). \end{aligned} \tag{2.11}$$

Subtracting (2.11) from (2.10) and noting that $\Phi_\alpha = \phi_{00} + O(\mu^2)$, we can express Φ in terms of Φ_α:

$$\Phi = \Phi_\alpha + \mu^2\left[(z_\alpha - z)\nabla \cdot (h\nabla\Phi_\alpha) + \tfrac{1}{2}(z_\alpha^2 - z^2)\nabla^2\Phi_\alpha\right] + O(\mu^4). \tag{2.12}$$

Substituting (2.12) into the mass conservation equation (2.6) and the dynamic free surface boundary condition (2.5) and neglecting $O(\epsilon\mu^2, \mu^4)$ terms, we obtain a new set of Boussinesq equations, called the modified Boussinesq equations, expressed in terms of the free surface displacement ζ and the velocity potential Φ_α on elevation $z = z_\alpha(x, y)$:

$$\begin{aligned} &\frac{\partial\zeta}{\partial t} + \nabla \cdot [(\epsilon\zeta + h)\nabla\Phi_\alpha] + \mu^2\nabla \cdot \left\{h\nabla\left[z_\alpha\nabla \cdot (h\nabla\Phi_\alpha)\right.\right. \\ &\quad \left.\left. + \frac{z_\alpha^2}{2}\nabla^2\Phi_\alpha\right] + \frac{h^2}{2}\nabla\left[\nabla \cdot (h\nabla\Phi_\alpha)\right] - \frac{h^3}{6}\nabla\nabla^2\Phi_\alpha\right\} = 0, \end{aligned} \tag{2.13}$$

$$\frac{\partial\Phi_\alpha}{\partial t} + \zeta + \frac{\epsilon}{2}(\nabla\Phi_\alpha)^2 + \mu^2\left[z_\alpha\nabla \cdot \left(h\nabla\frac{\partial\Phi_\alpha}{\partial t}\right) + \frac{z_\alpha^2}{2}\nabla^2\frac{\partial\Phi_\alpha}{\partial t}\right] = 0. \tag{2.14}$$

From (2.12), we have

$$\nabla\Phi_\alpha = \boldsymbol{u}_\alpha - \mu^2\left[\nabla \cdot (h\nabla\Phi_\alpha) + z_\alpha\nabla^2\Phi_\alpha\right]\nabla z_\alpha + O(\mu^4), \tag{2.15}$$

where $\boldsymbol{u}_\alpha = \nabla\Phi|_{z=z_\alpha}$ is the horizontal velocity at $z = z_\alpha$. Substituting (2.15) into the leading-order terms in (2.13) and in the gradient of (2.14) and replacing $\nabla\Phi_\alpha$ in the higher-order terms by $\boldsymbol{u}_\alpha$, one can show that the resulting equations are the alternative form of the modified Boussinesq equations derived by Nwogu (1993*a*), who also solved his equations numerically in the time domain (Nwogu 1993*a*, *b*).

Only two unknowns, Φ_α and ζ, appear in the modified Boussinesq equations (2.13) and (2.14) instead of three unknowns in the alternative form of the modified Boussinesq equations derived by Nwogu. Furthermore, (2.13) and (2.14) can be combined into one equation in terms of Φ_α. Therefore, in the remainder of this paper we shall carry out analyses and discussions based on (2.13) and (2.14).

3. Linear properties of the modified Boussinesq equations

In the case of constant depth, the corresponding linearized dimensional equations of (2.13) and (2.14) become (primes have been dropped)

$$\frac{\partial \zeta}{\partial t} + h\nabla^2 \Phi_\alpha + (\alpha + 1/3)h^3 \nabla^4 \Phi_\alpha = 0, \tag{3.1}$$

$$\frac{\partial \Phi_\alpha}{\partial t} + g\zeta + \alpha h^2 \nabla^2 \frac{\partial \Phi_\alpha}{\partial t} = 0, \tag{3.2}$$

where

$$\alpha = \tfrac{1}{2}(z_\alpha/h)^2 + (z_\alpha/h) \tag{3.3}$$

is a constant.

The phase velocity C and the group velocity C_g associated with the linearized modified Boussinesq equations (3.1) and (3.2) are given by

$$C^2 = \frac{\omega^2}{k^2} = gh\left[\frac{1-(\alpha+1/3)(kh)^2}{1-\alpha(kh)^2}\right], \tag{3.4}$$

$$C_g = \frac{\mathrm{d}\omega}{\mathrm{d}k} = C\left\{1 - \frac{(kh)^2/3}{\left[1-\alpha(kh)^2\right]\left[1-(\alpha+1/3)(kh)^2\right]}\right\}, \tag{3.5}$$

where k is the wavenumber and ω is the frequency. Expressions (3.4) and (3.5) have also been given by Nwogu (1993*a*). Comparing with those given by the linear Stokes theory over a range of depths from zero to one half of the equivalent deep-water wavelength λ_0 defined as $\lambda_0 = 2\pi g/\omega^2$, Nwogu (1993*a*) showed that the dispersion properties of the linearized modified Boussinesq equations strongly depend on the choice of the α value.

To extend the range of applicability of the modified Boussinesq equations, we define the sum of relative errors of the phase and group velocities over the range $0 \leqslant h/\lambda_0 \leqslant 0.5$ as

$$I_1(\alpha) = \int_0^{0.5} \left[(C/C_l - 1)^2 + (C_g/C_{gl} - 1)^2\right] \mathrm{d}(h/\lambda_0), \tag{3.6}$$

where C_l and C_{gl} are the phase and group velocities given by the linear Stokes theory.

Minimizing $I_1(\alpha)$, we find $\alpha = -0.3855$, which corresponds to the elevation $z_\alpha = -0.522h$ (see (3.3)). The maximum relative errors of the phase and group velocities over the range $0 \leqslant h/\lambda_0 \leqslant 0.5$ are 1.37% and 6.80%, respectively. We note that Nwogu (1993*a*) obtained a slightly smaller value for α, which is -0.390, by minimizing only the relative errors of the phase velocity.

Besides the phase velocity and group velocity, Madsen & Sørensen (1992) introduced 'linear shoaling gradient' as another quantity to measure the improvement of the new set of equations. For a train of monochromatic waves propagating over a mild slope, the linearized modified Boussinesq equations predict (through the WKBJ method) that the relative increase rate of the wave amplitude A due to shoaling is

$$\frac{1}{A}\frac{\mathrm{d}A}{\mathrm{d}h} = -\frac{S}{h}, \tag{3.7}$$

where S is the linear shoaling gradient and is expressed in terms of kh:

$$S(kh) = \frac{2\alpha(kh)^2(1-a_4)}{1-\alpha(kh)^2} - a_5, \tag{3.8}$$

with

$$a_1 = 1 + (\alpha + 1/3)(kh)^2 \left[\alpha(kh)^2 - 2\right], \tag{3.9}$$

$$a_2 = 1 + (\alpha + 1/3)(kh)^2 \left[5\alpha(kh)^2 - 6\right], \tag{3.10}$$

$$a_3 = 1 - 6(\alpha + 1/3)(kh)^2 + \left\{2\alpha + 5\alpha^2 + \tfrac{1}{3}\left[1 - (1 + 2\alpha)^{1/2}\right]\right\}(kh)^4, \tag{3.11}$$

$$a_4 = \frac{1}{2}\frac{1 - (2\alpha + 1)(kh)^2 + \alpha(\alpha + 1/3)(kh)^4}{1 - 2(\alpha + 1/3)(kh)^2 + \alpha(\alpha + 1/3)(kh)^4}, \tag{3.12}$$

$$a_5 = \frac{a_2 a_4 - a_3}{2a_1}. \tag{3.13}$$

On the other hand, the linear Stokes theory gives (Madsen & Sørensen 1992)

$$\frac{1}{A_l}\frac{\mathrm{d}A_l}{\mathrm{d}h} = -\frac{S_l}{h}, \tag{3.14}$$

where

$$S_l(k_l h) = \frac{2k_l h \sinh 2k_l h + 2(k_l h)^2(1 - \cosh 2k_l h)}{(2k_l h + \sinh 2k_l h)^2} \tag{3.15}$$

and k_l satisfies the dispersion relation

$$\omega^2 = g k_l \tanh k_l h. \tag{3.16}$$

From the dispersion relations (3.4) and (3.16), kh and $k_l h$ can be expressed in terms of h/λ_0. So can S and S_l. Integrating (3.7) and (3.14) with respect to h/λ_0, we obtain

$$\frac{A}{A_l} = \exp\left[\int_0^{h/\lambda_0} \frac{S_l(h'/\lambda_0) - S(h'/\lambda_0)}{h'/\lambda_0}\mathrm{d}(h'/\lambda_0)\right]. \tag{3.17}$$

We remark that the shoaling gradient is not a very good quantity to measure the linear shoaling effect. According to (3.17), the same deviation of the shoaling gradient has a different effect on the relative shoaling amplitude in different relative depth (has less effect as relative depth increases). The deviation of the shoaling gradient in intermediate depths and deep water exaggerates the actual difference of the shoaling amplitude.

Considering the shoaling effect in the determination of the α value, we minimize the following sum of relative errors:

$$I_2(\alpha, h/\lambda_0) = \int_0^{h/\lambda_0} \left[(C/C_l - 1)^2 + (C_g/C_{gl} - 1)^2 + (A/A_l - 1)^2\right] \mathrm{d}(h'/\lambda_0) \tag{3.18}$$

over the range $[0, 0.5]$ and obtain $\alpha = -0.3808$. Figure 1 shows the comparison between the phase velocity, group velocity and shoaling amplitude given by the linearized modified Boussinesq equations and those given by the linear Stokes theory for $\alpha = -0.3808$ (obtained by minimizing $I_2(\alpha, 0.5)$), $\alpha = -0.3855$ (obtained by minimizing $I_1(\alpha)$) and $\alpha = -2/5$ (with which (3.4) becomes the [2/2] Padé approximation to the fourth-order Taylor expansion of $gh\tanh kh/kh$). For $\alpha = -0.3808$ and $\alpha = -0.3855$, the relative errors of the phase and group velocities remain small over the entire interval $h/\lambda_0 \in [0, 0.5]$. However, the relative errors of the corresponding shoaling amplitude increase as depth increases (the shoaling effect imbedded in the modified Boussinesq equations is overestimated). When $h/\lambda_0 > 0.35$, the relative errors of the shoaling amplitude are in excess of 10% (see the solid line and dashed line in figure 1*c*). We could have improved the shoaling property by choosing a different α

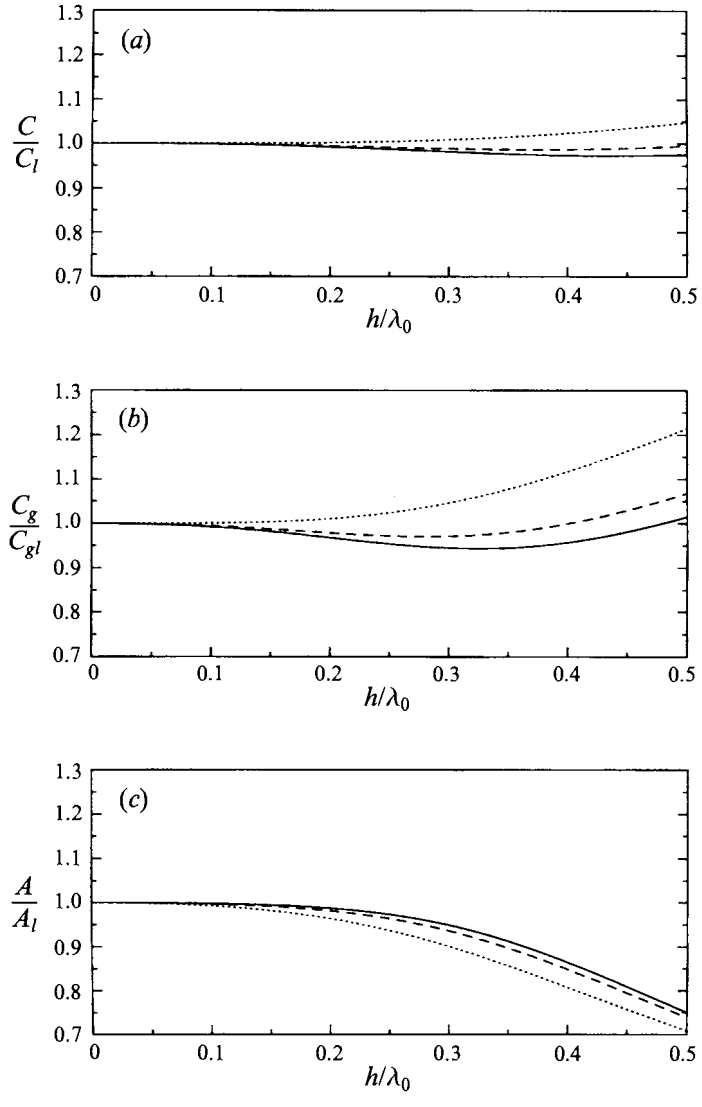

FIGURE 1. Comparison between (*a*) the phase velocity, (*b*) group velocity and (*c*) shoaling amplitude given by the linearized modified Boussinesq equations and those given by linear Stokes theory for different α values: ——, $\alpha = -0.3808$; - - -, $\alpha = -0.3855$; · · · ·, $\alpha = -2/5$.

value. But such an improvement is at a cost of increasing the errors of the phase and group velocities. If the shoaling effect is really important, the modified Boussinesq equations may not be extended to deep water ($h/\lambda_0 = 0.5$), but they can be extended to at least as deep as $h/\lambda_0 \approx 0.35$, the upper limit within which the relative errors of shoaling amplitude are less than 10%.

The value $\alpha = -0.3808$, obtained by minimizing the sum of the relatives errors of the phase velocity, group velocity and shoaling amplitude over the range $h/\lambda_0 \in [0, 0.5]$, gives the best overall improvement of the dispersion and shoaling properties. However, we would rather select $\alpha = -0.3855$ as the optimal value than $\alpha = -0.3808$. The reasons are as follows. Firstly, comparing the solid lines ($\alpha = -0.3808$) and dashed

lines ($\alpha = -0.3855$) in figure 1, one can see that although the shoaling property is improved when $\alpha = -0.3808$ is used, such an improvement is not dramatic and is accompanied by the degeneration of the dispersion properties. Secondly, if we minimize I_2 over the range $h/\lambda_0 \in [0, 0.35]$, we obtain $\alpha = -0.3858$, which is very close to $\alpha = -0.3855$. Thirdly, if the shoaling effect is not important, we only need to minimize I_1 and obtain $\alpha = -0.3855$, which gives the best overall dispersion properties over the range $h/\lambda_0 \in [0, 0.5]$.

Madsen & Sørensen (1992) chose their weighting factor $B = -(\alpha + 1/3) = 1/15$ (i.e. $\alpha = -2/5$) from the Padé approximation. Using this value, they found the shoaling gradient of their new Boussinesq equations agrees very well with that given by the linear theory. However, the error of the group velocity corresponding to this value may be too large (see the dotted line in figure 1*b*) for their Boussinesq equations to accurately describe the wave propagation stating from deep water.

In the above discussion the nonlinearity has been ignored. Because of shoaling, the wave amplitude and hence the nonlinearity, decrease as the depth (or μ^2) increases. Therefore, as long as the wave amplitude in the relatively deep water is so small that the Boussinesq approximation, i.e. $O(\epsilon) = O(\mu^2) \ll 1$, is still valid when the wave reaches the shallow-water region, the modified Boussinesq equations can be used to model wave propagation from relative deep water to shallow water (Nwogu 1993*a*, *b*).

We remark that although the modified Boussinesq equations are derived under the Boussinesq assumption, since the goal of deriving these equations is to extend their applicability into relatively deep water, we treat μ^2 as $O(1)$ from now on.

4. Parabolic models

The highest order of the spatial derivatives in the modified Boussinesq equations (2.13) and (2.14) is four. This makes the equations difficult to solve in the time domain. In this section we shall apply the parabolic approximation to the modified Boussinesq equations in the frequency domain and develop a small-angle model and an angular-spectrum model.

Considering regular waves, we can expand Φ_α and ζ as finite Fourier series in time:

$$\Phi_\alpha(x, y, t) = \frac{1}{2}\sum_{n=0}^{N} \phi_n(x, y)\mathrm{e}^{-\mathrm{i}n\omega t} + \text{c.c.}, \tag{4.1}$$

$$\zeta(x, y, t) = \frac{1}{2}\sum_{n=0}^{N} \zeta_n(x, y)\mathrm{e}^{-\mathrm{i}n\omega t} + \text{c.c.}, \tag{4.2}$$

where c.c. stands for the complex conjugate.

Substituting (4.1) and (4.2) into (2.13) and (2.14), we obtain

$$\mathrm{i}n\omega\zeta_n - \nabla\cdot(h\nabla\phi_n) - \frac{\epsilon}{2}\nabla\cdot\left\{\sum_{s=1}^{n-1}\zeta_s\nabla\phi_{n-s} + \sum_{s=1}^{N-n}\left[\bar{\zeta}_s\nabla\phi_{n+s} + \zeta_{n+s}\nabla\bar{\phi}_s\right]\right\} - \mu^2\nabla\cdot\boldsymbol{\rho}_n = 0, \tag{4.3}$$

$$\zeta_n = \mathrm{i}n\omega\phi_n + \mathrm{i}n\omega\mu^2 f_n - \frac{\epsilon}{4}\left[\sum_{s=1}^{n-1}\nabla\phi_s\cdot\nabla\phi_{n-s} + 2\sum_{s=1}^{N-n}\nabla\bar{\phi}_s\cdot\nabla\phi_{n+s}\right], \tag{4.4}$$

where

$$f_n(x,y) = z_\alpha \nabla \cdot (h\nabla\phi_n) + \frac{z_\alpha^2}{2}\nabla^2\phi_n = \alpha h^2\nabla^2\phi_n + z_\alpha \nabla h \cdot \nabla\phi_n, \tag{4.5}$$

$$\rho_n(x,y) = h\nabla f_n + \frac{h^2}{2}\nabla[\nabla\cdot(h\nabla\phi_n)] - \frac{h^3}{6}\nabla\nabla^2\phi_n. \tag{4.6}$$

In (4.3) and (4.4) the overbar is used to indicate the corresponding complex conjugate. The zeroth harmonic ϕ_0 has been ignored since it corresponds to a slowly varying steady state, i.e. $O(\nabla\phi_0) = O(\epsilon)$, which does not have any contribution to other harmonics up to $O(\epsilon)$.

To develop parabolic models, we first combine equations (4.3) and (4.4) into one equation in terms of velocity potential only. Substituting (4.4) into (4.3) and neglecting $O(\epsilon^2)$ terms, we obtain

$$\begin{aligned}\nabla\cdot(h\nabla\phi_n) + n^2\omega^2(\phi_n + \mu^2 f_n) + \mu^2\nabla\cdot\rho_n = -in\omega\frac{\epsilon}{4}\Bigg[\sum_{s=1}^{n-1}\nabla\phi_s\cdot\nabla\phi_{n-s} \\ + 2\sum_{s=1}^{N-n}\nabla\bar\phi_s\cdot\nabla\phi_{n+s}\Bigg] - i\omega\frac{\epsilon}{2}\nabla\cdot\Bigg\{\sum_{s=1}^{n-1}s(\phi_s+\mu^2 f_s)\nabla\phi_{n-s} \\ - \sum_{s=1}^{N-n}\left[s(\bar\phi_s+\mu^2\bar f_s)\nabla\phi_{n+s} - (n+s)(\phi_{n+s}+\mu^2 f_{n+s})\nabla\bar\phi_s\right]\Bigg\},\end{aligned} \tag{4.7}$$

where $n = 1,\ldots,N$. For the nth harmonic, the linear dispersion relation of (4.7) is

$$\frac{n^2\omega^2}{k_n^2} = h\frac{1-(\alpha+1/3)\mu^2(k_nh)^2}{1-\alpha\mu^2(k_nh)^2}. \tag{4.8}$$

When $n = 1$, the dimensional form of (4.8) is exactly the same as (3.4). Therefore, the improved dispersive characteristics of the modified Boussinesq equations with the optimal value of α are preserved. Alternatively, one may try to eliminate ϕ_n from (4.3) and (4.4) to obtain a combined equation for ζ_n. However, this cannot be done without introducing successive approximations in which μ^2 is assumed to be small. When the successive approximations are used, the improved dispersive properties of the new equations may be destroyed. This indeed happens when we eliminate the velocity potential from (4.3) and (4.4) and obtain an equation for the free surface displacement: the corresponding linear dispersion relation is given by (4.8) with $\alpha = 0$, which is worse than the linear dispersion relation of the conventional Boussinesq equations ($\alpha = -1/3$) (Wu 1979). In Nwogu's (1993*a*) paper, the alternative form of the modified Boussinesq equations is expressed in terms of the horizontal velocity components and the free surface displacement. Further approximations are necessary in order to combine the equations into one equation. If successive approximations are used to eliminate the velocity components in Nwogu's equations and obtain an equation for the free surface displacement, the resulting linear dispersion relation also corresponds to (4.8) with $\alpha = 0$. This is one of the primary reasons for using the velocity potential in this paper. The parabolic approximation can then be applied to the resulting equation for the velocity potential.

Assuming that the topography varies slowly, i.e. $h = h(\epsilon x, \epsilon y)$, we can further simplify (4.7) by ignoring $O(\epsilon^2)$ terms:

$$(\alpha+1/3)\mu^2h^3\nabla^4\phi_n + \beta_n\nabla^2\phi_n + n^2\omega^2\phi_n = -C_\alpha\mu^2h^2\nabla h\cdot\nabla\nabla^2\phi_n$$

$$- \tau_n \nabla h \cdot \nabla \phi_n - \mathrm{i}\omega \frac{\epsilon}{2} \sum_{s=1}^{n-1} s \left[2 \nabla \phi_s \cdot \nabla \phi_{n-s} + \alpha \mu^2 h^2 \nabla \nabla^2 \phi_s \cdot \nabla \phi_{n-s} \right.$$

$$\left. + (\phi_s + \alpha \mu^2 h^2 \nabla^2 \phi_s) \nabla^2 \phi_{n-s} \right] - \mathrm{i}\omega \frac{\epsilon}{2} \sum_{s=1}^{N-n} \left[n(2 \nabla \bar{\phi}_s \cdot \nabla \phi_{n+s} \right.$$

$$+ \alpha \mu^2 h^2 \nabla^2 \phi_{n+s} \nabla^2 \bar{\phi}_s) - s(\bar{\phi}_s \nabla^2 \phi_{n+s} + \alpha \mu^2 h^2 \nabla \nabla^2 \bar{\phi}_s \cdot \nabla \phi_{n+s})$$

$$\left. + (n+s)(\phi_{n+s} \nabla^2 \bar{\phi}_s + \alpha \mu^2 h^2 \nabla \nabla^2 \phi_{n+s} \cdot \nabla \bar{\phi}_s) \right] \quad (n = 1, \ldots, N), \tag{4.9}$$

where

$$\beta_n(x, y) = h + \alpha \mu^2 n^2 \omega^2 h^2, \tag{4.10}$$

$$\tau_n(x, y) = 1 + z_\alpha \mu^2 n^2 \omega^2, \tag{4.11}$$

$$C_\alpha = 1 + 5\alpha + (1 + 2\alpha)^{1/2}. \tag{4.12}$$

In (4.9), the first term on the left-hand side and the first term on the right-hand side come from $\mu^2 \nabla \cdot \boldsymbol{\rho}_n$ in (4.7).

Equation (4.9) is a set of weakly nonlinear coupled fourth-order elliptic equations with variable coefficients. The leading-order terms in (4.9), i.e. all terms on the left-hand side, describe the propagation of linear dispersive waves over a constant depth. The frequency dispersion is represented by the fourth-order derivative terms on the left-hand side of (4.9) as well as the second term in the coefficient β_n (see (4.10)) multiplied by $\nabla^2 \phi_n$. The first two terms on the right-hand side of (4.9) denote the effects related to the slope of the bathymetry, such as refraction and shoaling, whereas the rest of terms on the right-hand side are contributed by nonlinearity. For the one-dimensional case, (4.9) can be reduced to a set of fourth-order ordinary differential equations, which are similar to those obtained by Madsen & Sørensen (1993). We remark that the fourth-order derivative terms in (4.9) vanish when $\alpha = -1/3$, corresponding to the conventional Boussinesq equations. Once we solve (4.9) for $\phi_n(x, y)$ $(n = 1, \ldots, N)$, the free surface displacement $\zeta_n(x, y)$ $(n = 0, \ldots, N)$ can be computed immediately from (4.4). In the following subsections, we shall develop two parabolic models to approximate (4.9), namely, the small-angle model and the angular-spectrum model.

4.1. *Small-angle parabolic model*

For waves propagating primarily in the $\pm x$-direction, we assume that the variation of the wave field in the y-direction is small, i.e.

$$O\left(\frac{\partial^p \phi_n}{\partial y^p} \right) = O(\epsilon^{p/2}), \qquad p = 1, 2, 3, 4. \tag{4.13}$$

Moving terms containing y-derivatives to the right-hand side of (4.9), we obtain

$$(\alpha + 1/3) \mu^2 h^3 \frac{\partial^4 \phi_n}{\partial x^4} + \beta_n \frac{\partial^2 \phi_n}{\partial x^2} + n^2 \omega^2 \phi_n = \mathscr{T}_n, \tag{4.14}$$

where

$$\mathscr{T}_n = RHS - \beta_n \frac{\partial^2 \phi_n}{\partial y^2} - (\alpha + 1/3) \mu^2 h^3 \left(2 \frac{\partial^4 \phi_n}{\partial x^2 \partial y^2} + \frac{\partial^4 \phi_n}{\partial y^4} \right) \tag{4.15}$$

and RHS represents all terms on the right-hand side of (4.9).

Consider a special case – linear waves propagate in the x-direction over a constant depth. In this case, $\mathscr{T}_n = 0$ and the general solution to (4.14) can be expressed as

a linear combination of $\exp(\pm ik_n x)$ and $\exp(\pm k_n^e x)$. In other words, the whole wave field consists of a propagating wave field and a non-propagating wave field. This is also true for general cases.

To develop a small-angle parabolic model, we first separate the propagating wave field from the non-propagating wave field. Noting that $\mathscr{T}_n$ is $O(\epsilon)$, we treat (4.14) as a fourth-order (with respect to x) non-homogeneous 'ordinary' differential equation with $\mathscr{T}_n$ being the forcing term and rewrite (4.14) as two second-order (with respect to x) differential equations governing the propagating and non-propagating wave fields, respectively:

$$\phi_n = \phi_n^w + \phi_n^e, \tag{4.16}$$

$$\frac{\partial^2 \phi_n^w}{\partial x^2} = -k_n^2 \phi_n^w - \Gamma_n, \tag{4.17}$$

$$\frac{\partial^2 \phi_n^e}{\partial x^2} = (k_n^e)^2 \phi_n^e + \Gamma_n, \tag{4.18}$$

with

$$\Gamma_n = \frac{4(\alpha + 1/3)\mu^2 h^3}{W_n}\left(k_n^e \frac{\partial k_n^e}{\partial x}\frac{\partial \phi_n^e}{\partial x} - k_n \frac{\partial k_n}{\partial x}\frac{\partial \phi_n^w}{\partial x}\right) - \frac{\mathscr{T}_n}{W_n}, \tag{4.19}$$

$$W_n(x, y) = \beta_n - 2(\alpha + 1/3)\mu^2 h^3 k_n^2 = -(\alpha + 1/3)\mu^2 h^3 \left[k_n^2 + (k_n^e)^2\right] > 0, \tag{4.20}$$

where $\pm k_n$ and $\pm ik_n^e$ are the real and imaginary roots of the dispersion relation

$$(\alpha + 1/3)\mu^2 h^3 k^4 - \beta_n k^2 + n^2 \omega^2 = 0, \tag{4.21}$$

respectively. Thus,

$$k_n^2(x, y) = \frac{\beta_n - \left[\beta_n^2 - 4(\alpha + 1/3)\mu^2 n^2 \omega^2 h^3\right]^{1/2}}{2(\alpha + 1/3)\mu^2 h^3}, \tag{4.22}$$

$$(k_n^e)^2(x, y) = \frac{-\beta_n - \left[\beta_n^2 - 4(\alpha + 1/3)\mu^2 n^2 \omega^2 h^3\right]^{1/2}}{2(\alpha + 1/3)\mu^2 h^3}. \tag{4.23}$$

Equations (4.16)–(4.18) with Γ_n given by (4.19) are equivalent to (4.14) (note that we have neglected $O(\epsilon^2)$ terms in (4.19)).

Since the non-propagating wave field decays exponentially, for wave propagation problems, it usually can be neglected. If the non-propagating wave field is neglected, the original fourth-order differential equation (4.14) can be approximated by a second-order differential equation governing the propagating wave field (from (4.17) and (4.19))

$$\frac{\partial^2 \phi_n^w}{\partial x^2} = -k_n^2 \phi_n^w + \frac{4(\alpha + 1/3)\mu^2 h^3 k_n}{W_n}\frac{\partial k_n}{\partial x}\frac{\partial \phi_n^w}{\partial x} + \frac{\mathscr{T}_{hspace*-4ptn}}{W_n}. \tag{4.24}$$

We further split the propagating wave field into the forward and backward propagating wave fields and rewrite the second-order differential equation (4.24) as two first-order differential equations governing the forward and backward wave fields, respectively:

$$\phi_n^w = \phi_n^+ + \phi_n^-, \tag{4.25}$$

$$\frac{\partial \phi_n^+}{\partial x} = ik_n \phi_n^+ + \Theta_n, \tag{4.26}$$

$$\frac{\partial \phi_n^-}{\partial x} = -\mathrm{i}k_n\phi_n^- - \Theta_n, \tag{4.27}$$

with

$$\Theta_n = -\frac{P_n}{2k_nW_n}\frac{\partial k_n}{\partial x}\left(\phi_n^+ - \phi_n^-\right) - \frac{\mathrm{i}\mathscr{T}_n}{2k_nW_n}, \tag{4.28}$$

where

$$P_n(x,y) = \beta_n - 6(\alpha + 1/3)\mu^2h^3k_n^2. \tag{4.29}$$

Neglecting the backward wave field as a first approximation, we obtain

$$\frac{\partial \phi_n^+}{\partial x} = \mathrm{i}k_n\phi_n^+ - \frac{P_n}{2k_nW_n}\frac{\partial k_n}{\partial x}\phi_n^+ - \frac{\mathrm{i}\mathscr{T}_n}{2k_nW_n}. \tag{4.30}$$

Note that for the forward wave field, $\partial_x^p\phi_n^+ = (\mathrm{i}k_n)^p\phi_n^+ + O(\epsilon)$ $(p = 1,2,3,4)$ and the order of magnitude of each term in $\mathscr{T}_n$ is less than or equal to $O(\epsilon)$. Therefore, partial derivatives $\partial_x^p\phi_n^+$ in $\mathscr{T}_n$ can be replaced by $(\mathrm{i}k_n)^p\phi_n^+$. After the terms whose order of magnitude is less than $O(\epsilon)$ have been neglected, $\mathscr{T}_n$ becomes (superscript + has been dropped henceforth)

$$\mathscr{T}_n = -\mathrm{i}k_nR_n\frac{\partial h}{\partial x}\phi_n - W_n\frac{\partial^2\phi_n}{\partial y^2} - \mathrm{i}\omega\frac{\epsilon}{2}\left(\sum_{s=1}^{n-1}\hat{\sigma}_{ns}\phi_s\phi_{n-s} + \sum_{s=1}^{N-n}\hat{\gamma}_{ns}\bar{\phi}_s\phi_{n+s}\right), \tag{4.31}$$

where

$$R_n(x,y) = \tau_n - C_\alpha\mu^2h^2k_n^2, \tag{4.32}$$

$$\hat{\sigma}_{ns}(x,y) = sk_{n-s}\left[\alpha\mu^2h^2k_s^2(k_s + k_{n-s}) - (2k_s + k_{n-s})\right], \tag{4.33}$$

$$\hat{\gamma}_{ns}(x,y) = nk_sk_{n+s}(2 + \alpha\mu^2h^2k_sk_{n+s}) + sk_{n+s}(k_{n+s} + \alpha\mu^2h^2k_s^3) - (n+s)k_s(k_s + \alpha\mu^2h^2k_{n+s}^3). \tag{4.34}$$

Now we investigate how accurately the first-order equation (4.30) approximates the original fourth-order equation (4.14) for the forward wave field. When $\mathscr{T}_n = 0$, the general solution to (4.30) is

$$\phi_n = C_n\exp\left[\int_0^x\left(\mathrm{i}k_n - \frac{P_n}{2k_nW_n}\frac{\partial k_n}{\partial x}\right)\mathrm{d}x\right], \tag{4.35}$$

where C_n is a constant of integration. By direct substitution, one can observe that solution (4.35) is also a solution to (4.14) (up to $O(\epsilon)$). When $\mathscr{T}_n \neq 0$, we only need to check the particular solutions. For simplicity, we consider the constant-depth situation. Two types of forcing are examined: resonant and non-resonant forcing.

(*a*) For $k_{nx} = k_n$, $\mathscr{T}_n = A_n(y)\exp(\mathrm{i}k_{nx}x)$ represents resonant forcing (the forcing amplitude is allowed to vary in the y-direction). The particular solutions to (4.14) and (4.30) are given by

$$\phi_{np} = \frac{A_nx\exp(\mathrm{i}k_nx)}{2\mathrm{i}k_n\left[\beta_n - 2(\alpha + 1/3)\mu^2h^3k_n^2\right]}, \tag{4.36}$$

and

$$\phi_{np} = \frac{A_nx\exp(\mathrm{i}k_nx)}{2\mathrm{i}k_nW_n}, \tag{4.37}$$

respectively. According to the definition of W_n (see (4.20)), (4.37) is exactly the same as (4.36).

(*b*) For $k_{nx} \neq k_n$, $\mathscr{T}_n = A_n(y)\exp(\mathrm{i}k_{nx}x)$ represents non-resonant forcing. The particular solutions to (4.14) and (4.30) become

$$\phi_{np} = \frac{A_n \exp(\mathrm{i}k_{nx}x)}{(\alpha + 1/3)\mu^2 h^3 k_{nx}^4 - \beta_n k_{nx}^2 + n^2 w^2} = \frac{A_n \exp(\mathrm{i}k_{nx}x)}{(\alpha + 1/3)\mu^2 h^3 (k_{nx} - k_n)(k_{nx} + k_n)\left[k_{nx}^2 + (k_n^e)^2\right]}, \tag{4.38}$$

and

$$\phi_{np} = \frac{A_n \exp(\mathrm{i}k_{nx}x)}{2k_n W_n(k_n - k_{nx})} = \frac{A_n \exp(\mathrm{i}k_{nx}x)}{(\alpha + 1/3)\mu^2 h^3 (k_{nx} - k_n) 2k_n \left[k_n^2 + (k_n^e)^2\right]}, \tag{4.39}$$

respectively. Thus, the difference between solutions (4.38) and (4.39) is

$$\frac{A_n \exp(\mathrm{i}k_{nx}x)}{(\alpha + 1/3)\mu^2 h^3 (k_{nx} - k_n)} \left\{ \frac{1}{2k_n \left[k_n^2 + (k_n^e)^2\right]} - \frac{1}{(k_{nx} + k_n)\left[k_{nx}^2 + (k_n^e)^2\right]} \right\}.$$

Note that the expression in the bracket is proportional to $(k_{nx} - k_n)$. Therefore, the accuracy of the approximation depends on the difference between the x-component wavenumber of the forcing term k_{nx} and the characteristic wavenumber k_n. For resonant and near-resonant forcing, (4.30) approximates (4.14) very well. On the other hand, when the forcing wavenumber (more precisely, the x-component wavenumber) is far away from k_n, (4.30) is no longer a good approximation to (4.14). However, if we replace the denominator of the coefficient of the forcing term in (4.30), $2k_n W_n$, by $-(\alpha + 1/3)\mu^2 h^3 (k_{nx} + k_n)[k_{nx}^2 + (k_n^e)^2]$ (according to (4.20), these two expressions equal each other as $k_{nx} \to k_n$), the solution given by (4.30) is also a solution to (4.14) for any k_{nx} (regardless of whether k_{nx} is equal to k_n or not) in the constant-depth situation (for slowly varying depth, (4.30) will become a good approximation to (4.14)). The requirement for this replacement is that the x-component wavenumber of the forcing should be correctly estimated beforehand.

From (4.31), the forcing term $\mathscr{T}_n$ actually consists of linear terms and nonlinear terms. The x-component wavenumber of each term in (4.31) can be correctly estimated for waves propagating primarily in the $+x$-direction. In this situation, the x-component wavenumbers of the linear terms in (4.31) are close to k_n, whereas the x-component wavenumbers of the nonlinear terms $\phi_s \phi_{n-s}$ and $\bar{\phi}_s \phi_{n+s}$ in (4.31) are close to $(k_{n-s} + k_s)$ and $(k_{n+s} - k_s)$, respectively. Thus, there is no need to correct the coefficient of the linear terms since $k_{nx} \approx k_n$, i.e. the denominator $2k_n W_n$ in the last term in (4.30) remains the same for the first two linear terms in (4.31). However, since the differences between k_n and k_{nx} for the nonlinear terms $\phi_s \phi_{n-s}$ and $\bar{\phi}_s \phi_{n+s}$ in (4.31) (i.e. $k_{nx} - k_n \approx k_{n-s} + k_s - k_n$ and $k_{nx} - k_n \approx k_{n+s} - k_s - k_n$, respectively) may become large in intermediate depths and deep water, the denominator $2k_n W_n$ should be replaced by

$$-(\alpha + 1/3)\mu^2 h^3 (k_{n-s} + k_s + k_n)\left[(k_{n-s} + k_s)^2 + (k_n^e)^2\right]$$

and

$$-(\alpha + 1/3)\mu^2 h^3 (k_{n+s} - k_s + k_n)\left[(k_{n+s} - k_s)^2 + (k_n^e)^2\right],$$

respectively. In so doing, we finally obtain the small-angle parabolic model for the forward wave field ϕ_n, which consists of a set of weakly nonlinear coupled parabolic

equations with variable coefficients:

$$\frac{\partial \phi_n}{\partial x} = \mathrm{i}k_n\phi_n + \frac{\mathrm{i}}{2k_n}\frac{\partial^2\phi_n}{\partial y^2} - \frac{1}{2k_nW_n}\left(P_n\frac{\partial k_n}{\partial x} + k_nR_n\frac{\partial h}{\partial x}\right)\phi_n + \frac{\omega\epsilon}{2(\alpha+1/3)\mu^2h^3}\left\{\sum_{s=1}^{n-1}\frac{\hat{\sigma}_{ns}\phi_s\phi_{n-s}}{(k_{n-s}+k_s+k_n)\left[(k_{n-s}+k_s)^2+(k_n^e)^2\right]} + \sum_{s=1}^{N-n}\frac{\hat{\gamma}_{ns}\bar{\phi}_s\phi_{n+s}}{(k_{n+s}-k_s+k_n)\left[(k_{n+s}-k_s)^2+(k_n^e)^2\right]}\right\}, \tag{4.40}$$

where $n = 1,\ldots,N$.

In the case of constant depth, on substitution of the plane wave solution: $\phi_n = \exp[\mathrm{i}(k_{nx}x + k_{ny}y)]$, where k_{nx} and k_{ny} are the wavenumber components in the x- and y-direction respectively, the corresponding linearized equations of (4.9) and (4.40) give $k_{nx}^2 + k_{ny}^2 = k_n^2$ and $k_{nx}/k_n = 1 - \frac{1}{2}k_{ny}^2/k_n^2$, respectively. The angular limit of our small-angle model (4.40) turns out to be the same as that of the small-angle model to the mild-slope equation derived by Radder (1979) (the contribution from the variation of the topography and the nonlinearity are neglected), because both small-angle models use the same parabola $k_{nx}/k_n = 1 - \frac{1}{2}k_{ny}^2/k_n^2$ to approximate the circle $k_{nx}^2 + k_{ny}^2 = k_n^2$ in the (k_x, k_y)-plane. In practice, the bandwidth in the angular spectrum for the small-angle model should be $|\theta = \arctan(k_y/k_x)| \leqslant 30°$ (Chen & Liu 1994).

We can factor out the fast variable component in ϕ_n by introducing

$$\phi_n = \Psi_n \exp(\mathrm{i}k_n^* x) \tag{4.41}$$

into (4.40) and obtain

$$\frac{\partial \Psi_n}{\partial x} = \mathrm{i}(k_n - k_n^*)\Psi_n + \frac{\mathrm{i}}{2k_n}\frac{\partial^2\Psi_n}{\partial y^2} - \frac{1}{2k_nW_n}\left(P_n\frac{\partial k_n}{\partial x} + k_nR_n\frac{\partial h}{\partial x}\right)\Psi_n + \frac{\omega\epsilon}{2(\alpha+1/3)\mu^2h^3}\left(\sum_{s=1}^{n-1}\sigma_{ns}\Psi_s\Psi_{n-s} + \sum_{s=1}^{N-n}\gamma_{ns}\overline{\Psi}_s\Psi_{n+s}\right), \tag{4.42}$$

where

$$\sigma_{ns}(x,y) = \frac{\hat{\sigma}_{ns}\exp\left[\mathrm{i}(k_s^* + k_{n-s}^* - k_n^*)x\right]}{(k_{n-s}+k_s+k_n)\left[(k_{n-s}+k_s)^2+(k_n^e)^2\right]}, \tag{4.43}$$

$$\gamma_{ns}(x,y) = \frac{\hat{\gamma}_{ns}\exp\left[\mathrm{i}(k_{n+s}^* - k_s^* - k_n^*)x\right]}{(k_{n+s}-k_s+k_n)\left[(k_{n+s}-k_s)^2+(k_n^e)^2\right]}, \tag{4.44}$$

and $k_n^*(n = 1,\ldots,N)$ are a set of constant reference wavenumbers.

After solving (4.42) for $\Psi_n(x,y)$ $(n = 1,\ldots,N)$, we can obtain the free surface displacement $\zeta_n(x,y)$ by substituting (4.41) into (4.4).

4.2. *Angular-spectrum parabolic model*

To develop an angular-spectrum model to approximate (4.9) for multi-directional wave propagation, we first decompose the wave field into a series of wave modes including the entire discrete angular spectrum by the pseudospectral Fourier method (Chen & Liu 1994). Then, we apply the parabolic approximation to the governing equations for each wave mode. To decompose the wave field, we need to introduce a

reference depth $D(x)$, which varies only in the x-direction, and rewrite (4.9) as

$$(\alpha + 1/3)\mu^2 D^3 \nabla^4 \phi_n + B_n \nabla^2 \phi_n + n^2\omega^2 \phi_n = -U_n - \mathrm{i}\omega \frac{\epsilon}{2} V_n, \tag{4.45}$$

where

$$B_n(x) = D + \alpha\mu^2 n^2 \omega^2 D^2, \tag{4.46}$$

$$\begin{aligned} U_n(x,y) = {} & (\beta_n - B_n)\nabla^2\phi_n + (\alpha + 1/3)\mu^2(h^3 - D^3)\nabla^4\phi_n \\ & + C_\alpha \mu^2 h^2 \nabla h \cdot \nabla\nabla^2\phi_n + \tau_n \nabla h \cdot \nabla\phi_n, \end{aligned} \tag{4.47}$$

$$\begin{aligned} V_n(x,y) = {} & \sum_{s=1}^{n-1} s\left[2\,\nabla\phi_s \cdot \nabla\phi_{n-s} + \alpha\mu^2 h^2 \nabla\nabla^2\phi_s \cdot \nabla\phi_{n-s}\right. \\ & \left. + (\phi_s + \alpha\mu^2 h^2 \nabla^2\phi_s)\nabla^2\phi_{n-s}\right] \\ & + \sum_{s=1}^{N-n} \left[n(2\nabla\bar{\phi}_s \cdot \nabla\phi_{n+s} + \alpha\mu^2 h^2 \nabla^2\phi_{n+s}\nabla^2\bar{\phi}_s)\right. \\ & - s(\bar{\phi}_s \nabla^2\phi_{n+s} + \alpha\mu^2 h^2 \nabla\nabla^2\bar{\phi}_s \cdot \nabla\phi_{n+s}) \\ & \left. + (n+s)(\phi_{n+s}\nabla^2\bar{\phi}_s + \alpha\mu^2 h^2 \nabla\nabla^2\phi_{n+s} \cdot \nabla\bar{\phi}_s)\right]. \end{aligned} \tag{4.48}$$

We assume that the wave field in the alongshore direction (y-direction) is periodic with a period L. After a linear transformation mapping the interval $y \in [0, L]$ to $\tilde{y} \in [0, 2\pi]$ is taken, (4.45) becomes

$$\begin{aligned} & (\alpha + 1/3)\mu^2 D^3 \left[\frac{\partial^4\phi_n}{\partial x^4} + 2\Lambda_0 \frac{\partial^4\phi_n}{\partial x^2 \partial\tilde{y}^2} + \Lambda_0^2 \frac{\partial^4\phi_n}{\partial\tilde{y}^4}\right] \\ & + B_n \left[\frac{\partial^2\phi_n}{\partial x^2} + \Lambda_0 \frac{\partial^2\phi_n}{\partial\tilde{y}^2}\right] + n^2\omega^2\phi_n = -U_n - \mathrm{i}\omega\frac{\epsilon}{2}V_n, \end{aligned} \tag{4.49}$$

where

$$\Lambda_0 = (2\pi/L)^2. \tag{4.50}$$

Now we use trigonometric polynomials to interpolate $\phi_n(x, \tilde{y})$ in the $\tilde{y}$-direction at the following set of collocation points (Gottlieb, Hussaini & Orszag 1984):

$$\tilde{y}_j = \pi j/M, \qquad j = 0, \ldots, 2M-1, \tag{4.51}$$

$$\phi_n(x, \tilde{y}) = \sum_{j=0}^{2M-1} \phi_n^j(x) g_j(\tilde{y}), \tag{4.52}$$

where

$$\phi_n^j(x) = \phi_n(x, \tilde{y}_j), \quad g_j(\tilde{y}) = \frac{1}{2M}\sin[M(\tilde{y} - \tilde{y}_j)]\cot[(\tilde{y} - \tilde{y}_j)/2]. \tag{4.53}$$

The interpolants $g_j(\tilde{y})\,(j = 0, \ldots, 2M-1)$ are trigonometric polynomials of degree M and at each collocation point $\tilde{y}_m$, $g_j(\tilde{y}_m) = \delta_{jm}$. The pth-order ($p = 1, 2, 3, 4$) derivative of $\phi_n(x, \tilde{y})$ with respect to $\tilde{y}$, evaluated at the collocation $\tilde{y} = \tilde{y}_m$ is given by

$$\frac{\partial^p \phi_n(x, \tilde{y}_m)}{\partial\tilde{y}^p} = \sum_{j=0}^{2M-1} \phi_n^j(x) \frac{\mathrm{d}^p g_j(\tilde{y}_m)}{\mathrm{d}\tilde{y}^p} = \sum_{j=0}^{2M-1} [D_p]_{mj} \phi_n^j(x), \tag{4.54}$$

where

$$[D_p]_{mj} = \frac{\mathrm{d}^p g_j(\tilde{y}_m)}{\mathrm{d}\tilde{y}^p} \tag{4.55}$$

is a $2M \times 2M$ matrix. Specifically,

$$[D_1]_{mj} = \begin{cases} \frac{1}{2}(-1)^{m+j} \cot\left[(\tilde{y}_m - \tilde{y}_j)/2\right], & j \neq m \\ 0, & j = m \end{cases} \tag{4.56}$$

and

$$[D_2]_{mj} = \begin{cases} \frac{1}{2}(-1)^{m+j+1} \csc^2\left[(\tilde{y}_m - \tilde{y}_j)/2\right], & j \neq m \\ -(2M^2+1)/6, & j = m. \end{cases} \tag{4.57}$$

When $p > 2$, the pth-order spectral differentiation matrix $\boldsymbol{D}_p$ can be written as a power of $\boldsymbol{D}_2$ if p is even and as a power of $\boldsymbol{D}_1$ (or $\boldsymbol{D}_1$ times a power of $\boldsymbol{D}_2$) if p is odd.

From (4.56) and (4.57), $\boldsymbol{D}_1$ is a real antisymmetric matrix and $\boldsymbol{D}_2$ is a real symmetric matrix. Hence, $\boldsymbol{D}_{2p}$ is also a real symmetric matrix, whereas $\boldsymbol{D}_{2p+1}$ is a real antisymmetric matrix for $p \geqslant 1$.

Substituting (4.52) into (4.49), evaluating the resulting equation at each collocation point $\tilde{y} = \tilde{y}_m$ $(m = 0, \ldots, 2M-1)$ and noting (4.54), we obtain

$$\begin{aligned} &(\alpha + 1/3)\mu^2 D^3 \left\{ \frac{\mathrm{d}^4 \phi_n^m}{\mathrm{d}x^4} + 2\Lambda_0 \sum_{j=0}^{2M-1} [D_2]_{mj} \frac{\mathrm{d}^2 \phi_n^j}{\mathrm{d}x^2} + \Lambda_0^2 \sum_{j=0}^{2M-1} [D_4]_{mj} \phi_n^j \right\} \\ &\quad + B_n \left\{ \frac{\mathrm{d}^2 \phi_n^m}{\mathrm{d}x^2} + \Lambda_0 \sum_{j=0}^{2M-1} [D_2]_{mj} \phi_n^j \right\} + n^2 \omega^2 \phi_n^m = -U_n^m - \mathrm{i}\omega \frac{\epsilon}{2} V_n^m, \end{aligned} \tag{4.58}$$

where the superscript m denotes that the corresponding variable is evaluated at $\tilde{y} = \tilde{y}_m$. The dimensional forms of U_n^m and V_n^m are given in the Appendix. For a fixed n, equation (4.58) is a set of coupled ordinary differential equations for $\phi_n^m(x)$ $(m = 0, \ldots, 2M-1)$. The main coupling is provided by the spectral differentiation matrices $\boldsymbol{D}_2$ and $\boldsymbol{D}_4 = \boldsymbol{D}_2 \boldsymbol{D}_2$. Because $\boldsymbol{D}_2$ is symmetric, (4.58) (for a fixed n) can be almost decoupled (in the sense that the leading-order terms are decoupled but $O(\epsilon)$ terms are still coupled together) by decomposing the wave field into a series of wave modes, i.e. by introducing the transformation

$$\phi_n^m(x) = \sum_{q=0}^{2M-1} Q_{mq} \eta_n^q(x), \quad m = 0, \ldots, 2M-1, \tag{4.59}$$

where $\boldsymbol{Q}$ is a real orthogonal matrix such that

$$\boldsymbol{Q}^T \boldsymbol{D}_2 \boldsymbol{Q} = \frac{1}{\Lambda_0} \begin{bmatrix} -t_0^2 & & & \\ & -t_1^2 & & \\ & & \ddots & \\ & & & -t_{2M-1}^2 \end{bmatrix}. \tag{4.60}$$

The eigenvalues of $\boldsymbol{D}_2$: $-t_l^2/\Lambda_0$ $(l = 0, \ldots, 2M-1)$ and the transformation matrix $\boldsymbol{Q}$ can be given analytically (Chen & Liu 1994).

Substituting (4.59) into (4.58), multiplying the resulting equation by Q_{ml} and summing m from 0 to $(2M-1)$, we obtain

$$(\alpha + 1/3)\mu^2 D^3 \left[\frac{\mathrm{d}^4 \eta_n^l}{\mathrm{d}x^4} - 2t_l^2 \frac{\mathrm{d}^2 \eta_n^l}{\mathrm{d}x^2} + t_l^4 \eta_n^l \right] + B_n \left[\frac{\mathrm{d}^2 \eta_n^l}{\mathrm{d}x^2} - t_l^2 \eta_n^l \right]$$

$$+ n^2\omega^2\eta_n^l = -\sum_{m=0}^{2M-1} Q_{ml}\left[U_n^m + i\omega\frac{\epsilon}{2}V_n^m\right], \quad l = 0,\ldots,2M-1, \tag{4.61}$$

in which the orthogonality of $\boldsymbol{Q}$ and

$$\boldsymbol{Q}^T\boldsymbol{D}_4\boldsymbol{Q} = \boldsymbol{Q}^T\boldsymbol{D}_2\boldsymbol{Q}\boldsymbol{Q}^T\boldsymbol{D}_2\boldsymbol{Q} = \frac{1}{A_0^2}\begin{bmatrix} t_0^4 & & & \\ & t_1^4 & & \\ & & \ddots & \\ & & & t_{2M-1}^4 \end{bmatrix} \tag{4.62}$$

from (4.60) have been used.

To apply the parabolic approximation to (4.61), we need to impose another assumption on the topography: $(h - D) \sim O(\epsilon)$, i.e. the deviation of the actual depth from the reference depth is of the same order of magnitude as the typical wave amplitude; then all the terms on the right-hand side of (4.61) have the same order of magnitude of $O(\epsilon)$ (see (4.47) and (4.48)). Under this assumption, for a fixed n, (4.61) is a set of almost decoupled fourth-order ordinary differential equations for η_n^l ($l = 0,\ldots,2M-1$) which is similar to (4.14). Therefore, the same procedure used to derive the small-angle parabolic model can be applied to obtain a parabolic approximation to (4.61).

First, we separate propagating wave modes ($\langle\eta_n^l\rangle^w$) from non-propagating wave modes ($\langle\eta_n^l\rangle^e$):

$$\eta_n^l = \langle\eta_n^l\rangle^w + \langle\eta_n^l\rangle^e, \tag{4.63}$$

$$\frac{d^2\langle\eta_n^l\rangle^w}{dx^2} = -\left[K_n^2 - t_l^2\right]\langle\eta_n^l\rangle^w - \mathscr{P}_n^l, \tag{4.64}$$

$$\frac{d^2\langle\eta_n^l\rangle^e}{dx^2} = \left[(K_n^e)^2 + t_l^2\right]\langle\eta_n^l\rangle^e + \mathscr{P}_n^l, \tag{4.65}$$

with

$$\mathscr{P}_n^l = \frac{2(\alpha+1/3)\mu^2D^3}{F_n}\left[\frac{d(K_n^e)^2}{dx}\frac{d\langle\eta_n^l\rangle^e}{dx} - \frac{dK_n^2}{dx}\frac{d\langle\eta_n^l\rangle^w}{dx}\right] + \frac{1}{F_n}\sum_{m=0}^{2M-1} Q_{ml}\left(U_n^m + i\omega\frac{\epsilon}{2}V_n^m\right), \tag{4.66}$$

where $K_n(x)$ and $K_n^e(x)$ are given by

$$K_n^2 = \frac{B_n - \left[B_n^2 - 4(\alpha+1/3)\mu^2n^2\omega^2D^3\right]^{1/2}}{2(\alpha+1/3)\mu^2D^3}, \tag{4.67}$$

$$(K_n^e)^2 = \frac{-B_n - \left[B_n^2 - 4(\alpha+1/3)\mu^2n^2\omega^2D^3\right]^{1/2}}{2(\alpha+1/3)\mu^2D^3}, \tag{4.68}$$

and

$$F_n(x) = B_n - 2(\alpha+1/3)\mu^2D^3K_n^2 = -(\alpha+1/3)\mu^2D^3\left[K_n^2 + (K_n^e)^2\right] > 0. \tag{4.69}$$

Then, we neglect all non-propagating wave modes and approximate (4.61) by

$$\frac{d^2\langle\eta_n^l\rangle^w}{dx^2} = -\left[K_n^2 - t_l^2\right]\langle\eta_n^l\rangle^w + \frac{2(\alpha+1/3)\mu^2D^3}{F_n}\frac{dK_n^2}{dx}\frac{d\langle\eta_n^l\rangle^w}{dx}$$

$$-\frac{1}{F_n}\sum_{m=0}^{2M-1} Q_{ml}\left(U_n^m + \mathrm{i}\omega\frac{\epsilon}{2}V_n^m\right). \tag{4.70}$$

We further split the propagating wave modes into forward and backward propagating wave modes:

$$\langle\eta_n^l\rangle^w = \langle\eta_n^l\rangle^+ + \langle\eta_n^l\rangle^-, \tag{4.71}$$

$$\frac{\mathrm{d}\langle\eta_n^l\rangle^+}{\mathrm{d}x} = \mathrm{i}(K_n^2 - t_l^2)^{1/2}\langle\eta_n^l\rangle^+ + \mathscr{S}_n^l, \tag{4.72}$$

$$\frac{\mathrm{d}\langle\eta_n^l\rangle^-}{\mathrm{d}x} = -\mathrm{i}(K_n^2 - t_l^2)^{1/2}\langle\eta_n^l\rangle^- - \mathscr{S}_n^l, \tag{4.73}$$

with

$$\mathscr{S}_n^l = -\frac{E_{nl}}{4(K_n^2 - t_l^2)F_n}\frac{\mathrm{d}K_n^2}{\mathrm{d}x}\left(\langle\eta_n^l\rangle^+ - \langle\eta_n^l\rangle^-\right) + \frac{\mathrm{i}}{2F_n(K_n^2 - t_l^2)^{1/2}}\sum_{m=0}^{2M-1} Q_{ml}\left(U_n^m + \mathrm{i}\omega\frac{\epsilon}{2}V_n^m\right), \tag{4.74}$$

where

$$E_{nl}(x) = B_n - 2(\alpha + 1/3)\mu^2 D^3(3K_n^2 - 2t_l^2). \tag{4.75}$$

In the present study we assume that the backward propagating wave field is negligible. The governing equation (4.72) for the forward propagating wave modes then becomes (superscript + has been dropped henceforth):

$$\frac{\mathrm{d}\eta_n^l}{\mathrm{d}x} = \left[\mathrm{i}(K_n^2 - t_l^2)^{1/2} - \frac{E_{nl}}{4F_n(K_n^2 - t_l^2)}\frac{\mathrm{d}K_n^2}{\mathrm{d}x}\right]\eta_n^l + \frac{\mathrm{i}}{2F_n(K_n^2 - t_l^2)^{1/2}}\sum_{m=0}^{2M-1} Q_{ml}\left(U_n^m + \mathrm{i}\omega\frac{\epsilon}{2}V_n^m\right). \tag{4.76}$$

In the expression for $(U_n + \mathrm{i}\omega\epsilon V_n/2)$ (see (4.47) and (4.48)), the order of magnitude of all known coefficients is $O(\epsilon)$. Therefore, $\mathrm{d}^p\phi_n^m/\mathrm{d}x^p$ $(p = 1, 2, 3)$ in the expression for $(U_n^m + \mathrm{i}\omega\epsilon V_n^m/2)$ can be approximated as

$$\frac{\mathrm{d}^p\phi_n^m}{\mathrm{d}x^p} = \sum_{q=0}^{2M-1} Q_{mq}\frac{\mathrm{d}\eta_n^q}{\mathrm{d}x} \approx \sum_{q=0}^{2M-1} \mathrm{i}^p(K_n^2 - t_q^2)^{p/2}Q_{mq}\eta_n^q. \tag{4.77}$$

Now all terms on the right-hand side of (4.76) can be expressed in terms of η_n^q $(q = 0,\ldots,2M-1; n = 1,\ldots,N)$ and do not involve the derivatives of η_n^q. Because the terms on the right-hand side of (4.61) are very complicated, we do not pursue a similar justification to that for the small-angle model.

Note that for the nth harmonic, the propagation direction of each forward wave mode η_n^l is arctan $[t_l/(K_n^2 - t_l^2)^{1/2}]$ measured from the $+x$-direction. Equation (4.76) with (4.59) is called the 'angular-spectrum parabolic model', because for each harmonic, the wave field at each collocation point consists of contributions from $2M$ forward wave modes whose propagation directions cover the range from $-90°$ to $90°$, i.e. the upper half of the angular spectrum. By solving (4.76) numerically for $\eta_n^l(x)$ $(l = 0,\ldots,2M-1; n = 1,\ldots,N)$ (e.g. Runge–Kutta method), we can find the velocity potential for each harmonic $\phi_n(x, y)$ $(n = 1,\ldots,N)$ from (4.59) and the corresponding free surface elevation $\zeta_n(x, y)$ $(n = 0,\ldots,N)$ from (4.4).

5. Numerical examples

Several numerical examples are given in this section to demonstrate the applicability of the modified Boussinesq equations as well as the parabolic approximation models. For all numerical examples, the optimal value of $\alpha = -0.3855$ is used.

5.1. *Small-angle parabolic model*

Whalin (1971) conducted a series of laboratory experiments concerning wave focusing over a slowly varying topography. The wave tank was 25.603 m long and 6.096 m wide. In the middle portion of the wave tank (7.622 m $< x <$ 15.242 m), eleven semicircular steps were evenly spaced and led to the shallower portion of the channel.

The equation approximating the topography is given as follows (Whalin 1971):

$$h(x,y) = \begin{cases} 0.4572, & 0 \leqslant x \leqslant 10.67 - G, \\ 0.4572 + \frac{1}{25}(10.67 - G - x), & 10.67 - G \leqslant x \leqslant 18.29 - G, \\ 0.1524, & 18.29 - G \leqslant x \leqslant 25.0, \end{cases} \tag{5.1}$$

where

$$G(y) = [y(6.096 - y)]^{1/2} \qquad (0 \leqslant y \leqslant 6.096). \tag{5.2}$$

In both (5.1) and (5.2), all variables are measured in metres. The bottom topography was symmetric with respect to the centreline of the wave tank $y = 3.048$ m. A wavemaker was installed at the deeper portion of the channel where the water depth was 0.4572 m. Three sets of experiments were conducted for periods $T = 1.0$, 2.0 and 3.0 s, respectively. Different wave amplitudes were generated for each wave period.

Several mathematical models have been developed and applied to simulate Whalin's experiments. Using the second-order Stokes theory, Liu & Tsay (1984) derived a model equation, which is a nonlinear Schrödinger equation with variable coefficients. They produced numerical results for wave periods of 1 and 2 s. Because the second-order Stokes wave theory was used, their model is unable to obtain more than two harmonics and is not valid for long waves, e.g. the $T = 3.0$ s cases. Liu *et al.* (1985) discussed two models for nonlinear refraction-diffraction of waves in shallow water: the conventional Boussinesq equations and the Kadomtsev–Petviashvili (KP) equation. They presented numerical results for the wave period of 3 s. These two models are restricted to shallow water and can not be extended to deal with intermediate depth cases, e.g. the $T = 1.0$ and 2.0 s cases in Whalin's experiments. Rygg (1988) solved the conventional Boussinesq equations directly with a line by line iterative method and compared his numerical results with Whalin's experimental data for the cases of $T = 2.0$ and 3.0 s. Solving Boussinesq-type equations in the time domain, Madsen & Sørensen (1992) and Nwogu (1993*b*) claimed that the new form of the Boussinesq equations they derived is capable of simulating all cases in Whalin's experiments correctly.

We now apply our small-angle parabolic model to all cases in Whalin's experiments: $T = 1.0, 2.0$ and 3.0 s, which in the deeper portion of the channel correspond to relative depth $h/\lambda_0 = 0.2931$, 0.0733 and 0.0326, respectively. The pseudospectral Chebyshev method is employed to solve the small-angle model (Chen 1995). Because of the symmetry of the problem with respect to the centreline of the wave tank, the computational domain only consists of one half of the wave tank. No-flux boundary conditions are used along the right-hand sidewall and the centreline of the wave tank. The computational domain in the x-direction starts from the wavemaker $x = 0$ and ends at $x = 25$ m. Wavenumbers of each harmonic at $x = 0$ are used as reference wavenumbers k_n^*.

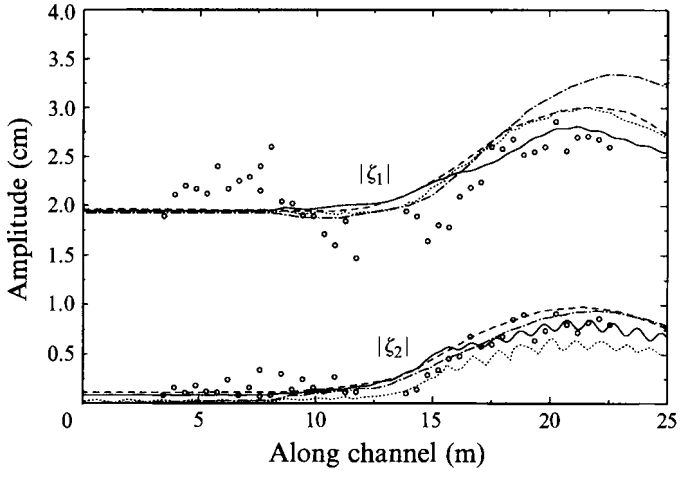

FIGURE 2. Wave amplitude along the centreline of the wave tank for $T = 1.0$ s and $a_0 = 1.95$ cm. ——, Small-angle model; – · –, results given by Nwogu (1993*b*); · · · ·, results given by Madsen & Sørensen (1992); - - -, results given by Liu & Tsay (1984); ○ ○ ○, experimental data (Whalin 1971).

For the $T = 2.0$ and 3.0 s cases, the linear monochromatic boundary conditions are used as initial conditions at $x = 0$. Numerical results are practically identical to those given by Madsen & Sørensen (1992) and Rygg (1988) and agree with the experimental data quite well. Comparisons between numerical results and experimental data are not presented here. For the period $T = 1.0$ s and amplitude $a_0 = 1.95$ cm case, which the conventional Boussinesq equations are unable to predict correctly, the comparison between the present model results and the experimental data (Whalin 1971) is shown in figure 2. Only two harmonics are considered and seven collocation points in the y-direction are used. The marching step in x-direction is 0.1 cm. In this case, because the phase mismatch between the free and bound second harmonic is not small, the second-order boundary condition is used as the initial condition to remove the spurious spatial variation of the incident wave amplitude (Madsen & Sørensen 1993), i.e. to get rid of the parasitic free second harmonic in the incident wave. From figure 2, one can see that in spite of the scattering in the experimental data, the model results agree with the experimental data reasonably well, especially in the focal zone. The oscillation in the second harmonic (first observed by Madsen & Sørensen 1992) indicates that the free second harmonic is released on the top of the shelf (where the relative depth based on the free second harmonic is 0.3908) due to the abrupt change of the topography. The free and bound second harmonic propagate not only with different speeds but also in different directions (Madsen & Sørensen 1992).

For comparison, the results given by Liu & Tsay (1984), Madsen & Sørensen (1992) and Nwogu (1993*b*) are also plotted in figure 2. In the focal zone, Nwogu's results slightly overestimate the first harmonic, whereas Madsen & Sørensen's results slightly underestimate the second harmonic. The oscillation phenomenon, which is predicted by our small-angle model and Madsen & Sørensen's extended Boussinesq equations, however, was not shown in Nwogu's results (it is understandable that Liu & Tsay's numerical results did not show this phenomenon, because the second-order Stokes theory they used excludes the free second harmonic). According to the Stokes second-order theory, our modified Boussinesq equations and the extended Boussinesq equations given by Madsen & Sørensen, the amplitudes of the bound

second harmonic in the incident wave are 0.0950, 0.0833, 0.0276 cm, respectively (Chen 1995). The second-order amplitude of the incident wave is slightly underestimated in the modified Boussinesq equations, whereas it is much more underestimated in Madsen & Sørensen's new set of equations. This is why the incident wave can be treated as a linear wave in their model (they used the linear monochromatic boundary condition at the incident boundary) and the amplitude of the second harmonic they obtained is underestimated in the focal zone. Nwogu (1993*b*) also used the first-order boundary condition at the incident boundary. We remark that if the first-order boundary condition at the incident boundary is used, the spurious free second harmonic having the same amplitude as the bound second harmonic, which cannot be neglected in this case, will be released in the constant-depth region ($h = 0.4752$ m). In this region, the modified Boussinesq equations are unable to describe the free second harmonic accurately because the relative depth based on the free second harmonic ($h/\lambda_0 = 1.1725$) is far away from the range of the applicability of the equations, which is $h/\lambda_0 \in [0, 0.5]$. Therefore, the second-order boundary condition should be used to get the correct results in this case.

Similar results are obtained for the $T = 1.0$ s and $a_0 = 0.75$ cm case, which are not repeated here.

5.2. *Angular-spectrum parabolic model*

For normal incident waves propagating over a one-dimensional bottom $h = h(x)$, the results given by the angular-spectrum model are identical to those given by the small-angle model without modifying the coefficients of the nonlinear terms, i.e. (4.30) with (4.31). Thus, the angular-spectrum can be applied only to cases with a nearly triad resonance ($k_n \approx k_{n\pm s} \mp k_s$), e.g. in shallow water. We now apply the angular-spectrum model to study the refraction of a cnoidal wavetrain and the oblique interactions of two identical cnoidal wavetrains in shallow water.

To construct a cnoidal wavetrain, an infinite number of harmonics should be used. In actual numerical integration, we can, however, only include a finite number of harmonics. Yoon & Liu (1989) demonstrated that if the first several harmonics of the cnoidal wave solution to the KdV equation are retained as the input to their parabolic model, the resulting cnoidal wavetrain does not have a uniform amplitude. An alternative approach, which we shall adopt, is to find initial conditions for the numerical integration that lead to permanent cnoidal wave forms in the constant-depth region (Kirby 1991).

We expand the velocity potential Φ_α and the free surface displacement ζ in finite Fourier series

$$\Phi_\alpha(x,t) = \sum_{n=1}^{N} \varphi_n \sin[n(kx - \omega t)], \qquad \zeta(x,t) = \sum_{n=1}^{N} a_n \cos[n(kx - \omega t)], \tag{5.3}$$

which represent a uniform cnoidal wave propagating in the $+x$-direction with φ_n, a_n and k to be determined. A set of nonlinear algebraic equations for φ_n, a_n and k can be derived from the small-angle parabolic model without modifying the coefficients of the nonlinear terms, the expression for the free surface displacement, (4.4), and the relation between the wave height of a uniform cnoidal wave and the amplitude of each harmonic (Chen 1995). The Newton–Raphson method is used to obtain φ_n, a_n and k for given wave period T, wave height H and water depth h.

The initial conditions of a uniform cnoidal wave with an angle of incidence θ_0 for

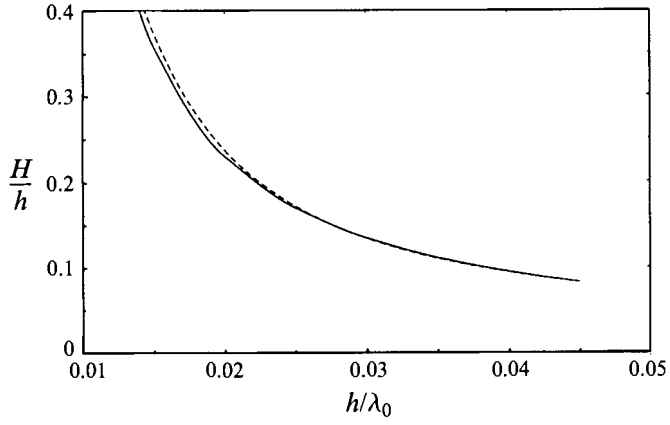

FIGURE 3. Refraction of a cnoidal wave over a mild-slope plain beach. ——, Cnoidal wave refraction theory (Skovgaard & Petersen 1977); - - -, angular-spectrum model.

the angular-spectrum model are given by

$$\phi_n(0, y) = -\mathrm{i}\varphi_n \exp(\mathrm{i}nky \sin\theta_0), \qquad \eta_n^l(0) = \sum_{m=0}^{2M-1} Q_{ml}\phi_n^m(0). \tag{5.4}$$

When $\theta_0 \neq 0$, the periodicity condition in the y-direction requires

$$L = \frac{2\pi}{k \sin\theta_0} p, \tag{5.5}$$

where $p(\neq 0)$ is an arbitrary integer.

We remark that although φ_n $(n = 1, \ldots, N)$ and k in (5.4) are determined based on the small-angle model, numerical tests show that when (5.4) is used as the initial input, the angular-spectrum model maintains the uniformity of the cnoidal wave as it propagates towards the shoreline.

Skovgaard & Petersen (1977) presented a theoretical solution of the refraction of cnoidal waves over a gently sloping bathymetry whose contour lines are straight and parallel to the shoreline. With the basic assumption that the energy flux is a constant between adjacent wave orthogonals, they derived two nonlinear algebraic equations for the wave height and the elliptic parameter.

To compare our angular-spectrum model with the cnoidal wave refraction theory, we have chosen the top row in table 1 in Skovgaard & Petersen's (1977) paper as the incident wave parameters:

$$h_0/\lambda_0 = 0.045, \qquad H_0/h_0 = 0.0826, \qquad \theta_0 = 25.9°, \tag{5.6}$$

where H_0 and h_0 are the wave height and water depth at $x = 0$, respectively, and $\lambda_0 = gT^2/2\pi$ is the deep-water wavelength. For incident cnoidal wave with period $T = 3.0$ s, the deep water wavelength is $\lambda_0 = 14.04$ m and from (5.6) the water depth and wave height are $h_0 = 0.6317$ m and $H_0 = 0.0522$ m, respectively. The topography is given by

$$h(x) = D(x) = 0.6317 - 0.03x. \tag{5.7}$$

$N = 7$ and $M = 16$ are used and the numerical integration is carried out from $x = 0$ to $x = 17$ m with a marching step $\Delta x = 0.1$ m. The computational domain in

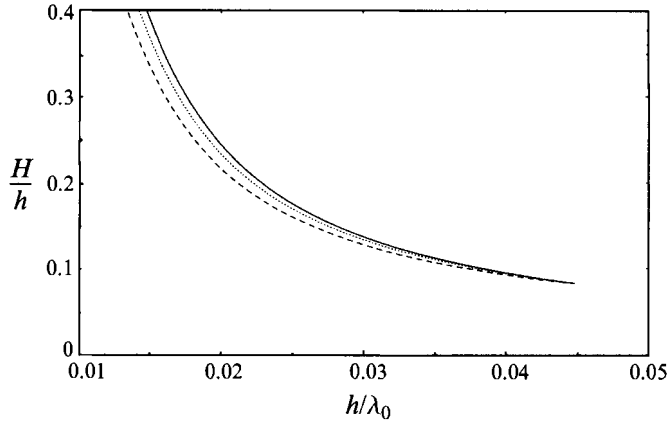

FIGURE 4. Dimensionless wave height H/h as a function of dimensionless water depth h/λ_0 for different angles of incidence: ——, $\theta_0 = 0°$; · · · ·, $\theta_0 = 30°$; - - -, $\theta_0 = 45°$.

the y-direction is $L = 16.35$ m ($p = 1$ in (5.5)). The comparison between numerical results and theoretical results is shown in figure 3. The agreement is very satisfactory, especially when the nonlinearity is not too strong. When the beach slope, 0.03 (in (5.7)), is replaced by a gentler slope, 0.025, numerical results do not change. This confirms the assumption of the cnoidal wave refraction theory that the wave height is independent of the slope of the bathymetry (as long as it is very mild).

For the same wave conditions, figure 4 shows the dimensionless wave height H/h as a function of the dimensionless water depth h/λ_0 for different angles of incidence: $\theta_0 = 0°$, $\theta_0 = 30°$ and $\theta_0 = 45°$. The wave height decreases as the angle of incidence increases.

Comparing the genus 2 solution to the KP equation with the solution based on the linear superposition of two cnoidal waves, Hammack, Scheffner & Segur (1989) showed the importance of nonlinear interactions between two identical cnoidal waves propagating over a constant depth with directed wave angles $\pm\theta_0$. The KP equation can only correctly describe weakly nonlinear and dispersive wave propagation over a constant depth with weak transversal modulation. Although the KP equation can be extended to deal with cases with a slowly varying topography (Chen & Liu 1995), for large directed wave angle, e.g. $\theta_0 \geqslant 30°$, all KP-type equations become inadequate for modelling weakly nonlinear and dispersive wave propagation. In this situation, one may use the angular-spectrum model instead.

We now apply the angular-spectrum model to study the influence of the directed wave angle $\pm\theta_0$ on the oblique interaction of two identical cnoidal waves propagating over a constant depth and a slope connecting two constant depths. The wave parameters used in our computations are very close to those of Hammack *et al.*'s experiment (KP1515 in table 1 in their paper): $T = 2.55$ s and $H = 0.02$ m. The incident wavelength is 4.25 m. Two different directed angles are considered: $\theta_0 = 22.5°$ and $\theta_0 = 45°$, which represent small and large directed wave angles respectively. $N = 5$, $M = 25$, $\Delta x = 0.1$ m and $p = 2$ are used in numerical computations. The domain of computation in the y-direction covers two spatial periods.

Figures 5(*a*) and 5(*b*) show the contour plots of the free surface displacement for the nonlinear interaction and linear superposition of two cnoidal waves propagating over a constant depth $h = 0.3$ m with directed angles $\theta_0 = \pm 45°$ and $\theta_0 = \pm 22.5°$,

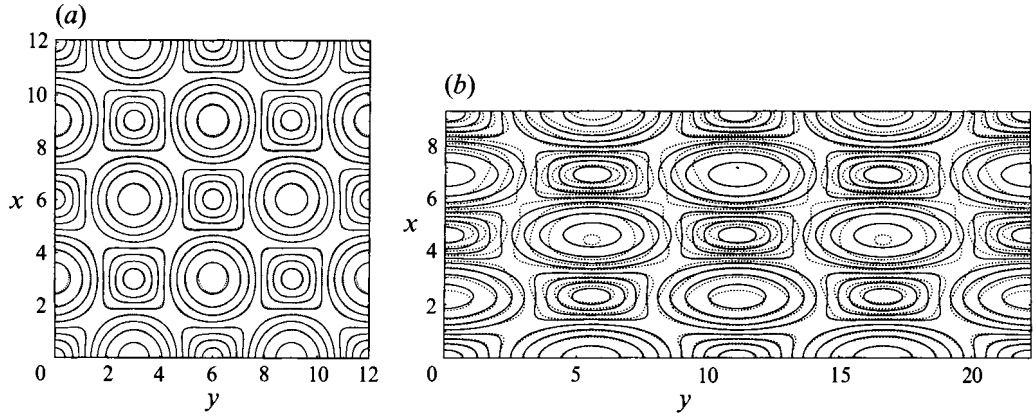

FIGURE 5. Contour plots of $\zeta(x, y, t)$ for linear superposition and nonlinear interaction of two identical cnoidal waves with directed wave angles (*a*) $\theta_0 = \pm 45°$, (*b*) $\theta_0 = \pm 22.5°$ at time $t = nT(n = 0, 1, \ldots)$. ——, Linear superposition; · · · ·, nonlinear interaction.

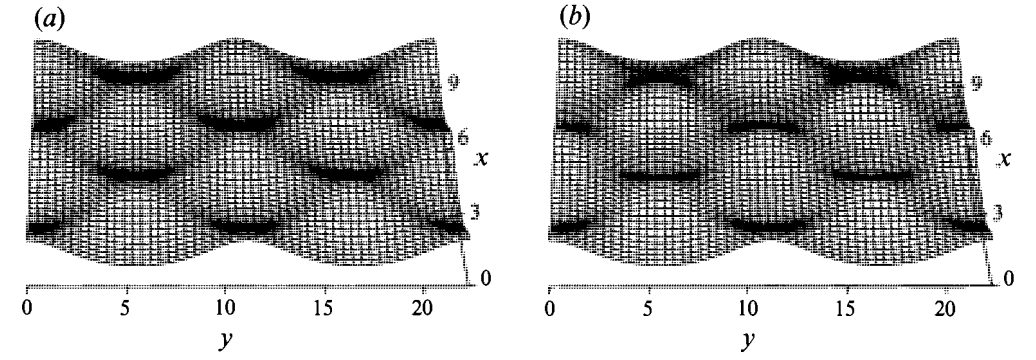

FIGURE 6. A perspective view of the free surface displacement for (*a*) linear superposition, (*b*) nonlinear interaction of two identical cnoidal wavetrains with directed wave angle $\theta_0 = \pm 22.5°$ at time $t = nT(n = 0, 1, \ldots)$.

respectively. The values of contour lines are from −1.5 cm to 2.0 cm with an increment of 0.5 cm. In figure 5(*a*), for large directed wave angles, the difference between the nonlinear solution and the linear-superposition solution is very small. On the other hand, for small directed wave angles, figure 5(*b*) shows that the difference is quite large and the nonlinear numerical solution evolves along the $+x$-direction. From the perspective pictures shown in figures 6(*a*) and 6(*b*), we observe that for small directed wave angles the nonlinear interaction increases the length of a crest. This agrees with the experimental observation (Hammack *et al.* 1989).

In his study of Mach reflection of a cnoidal wave from a vertical wall, Kirby (1990) showed that if the angle of incidence is small, a Mach stem evolves along the reflected wall. In contrast, when the angle of incidence is about 45°, the wave field exhibits almost a regular reflection pattern. This is consistent with our numerical results. Therefore, we may draw a conclusion that when the directed angle of two identical cnoidal waves propagating over a constant depth is large, the nonlinear interaction is weak and the wave field exhibits a nearly linearly superimposed wave pattern.

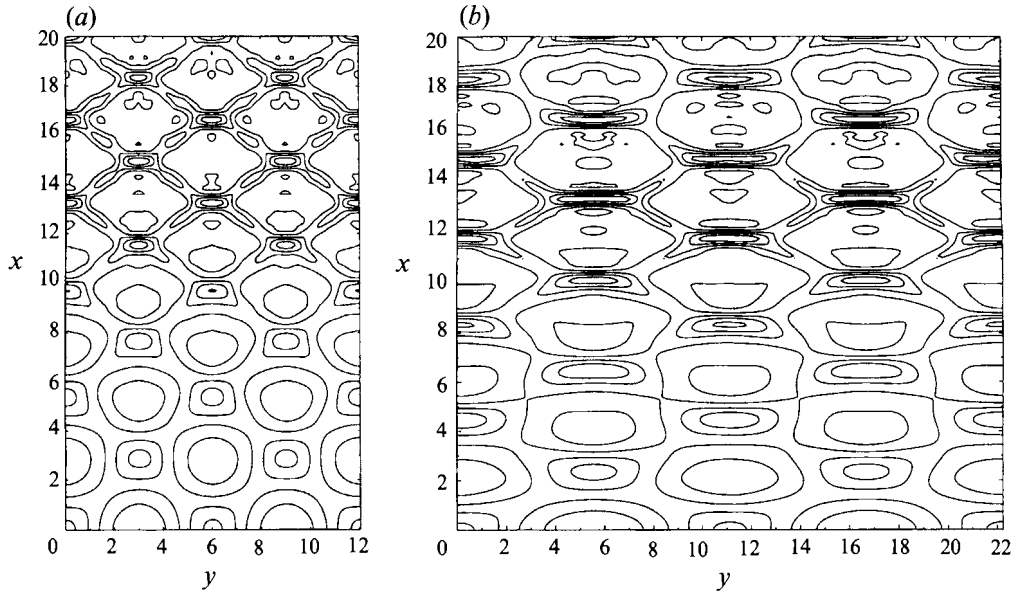

FIGURE 7. Contour plot of the free surface displacement for two cnoidal waves propagating over a slope with directed wave angles (*a*) $\theta_0 = \pm 45°$, (*b*) $\theta_0 = \pm 22.5°$ at time $t = nT (n = 0, 1, \ldots)$.

For the same incident wave conditions, figures 7(*a*) and 7(*b*) show the contour plots of the free surface displacement of two identical cnoidal waves with different directed angles propagating over a slope connecting two constant depths:

$$h(x) = \begin{cases} 0.3, & x \leqslant 0, \\ 0.3 - 0.015x, & 0 < x \leqslant 12, \\ 0.12, & x > 12. \end{cases} \tag{5.8}$$

The values of contour lines are -1, 0, 1, 2 and 3 cm. Figures 8(*a*) and 8(*b*) show the corresponding three-dimensional plots. From these figures, one can see that as the depth decreases, the nonlinearity increases and the crests of the surface displacement become longer, flatter and narrower. This tendency eventually leads to the formation of a hexagonal wave pattern. These features are also observed in the field (see figure 3 in Akylas' 1994 paper) and in the laboratory (Hammack *et al.* 1989). For $\theta_0 = \pm 45°$, the hexagonal pattern develops in the shallower constant-depth region (i.e. $x > 12$ m), whereas for $\theta_0 = \pm 22.5°$, it develops just before the end of the slope. The horizontal sides of the hexagons for $\theta_0 = \pm 22.5°$ are much longer than those for $\theta_0 = \pm 45°$. The hexagonal wave pattern for $\theta_0 = \pm 45°$ is more stable than that for $\theta_0 = \pm 22.5°$. But eventually all these hexagons will deform and disappear in the shallower constant-depth region as the waves propagate toward the shoreline.

6. Concluding remarks

We have formally derived the modified Boussinesq equations in terms of the velocity potential, $\Phi_\alpha(x, y, t)$, evaluated on an arbitrary elevation $z = z_\alpha(x, y)$, and the free surface displacement. We have showed that when Φ_α is evaluated at $z = -0.522h$, the corresponding modified Boussinesq equations have almost the same dispersive behaviour as that of the first-order Stokes waves for water depths ranging from

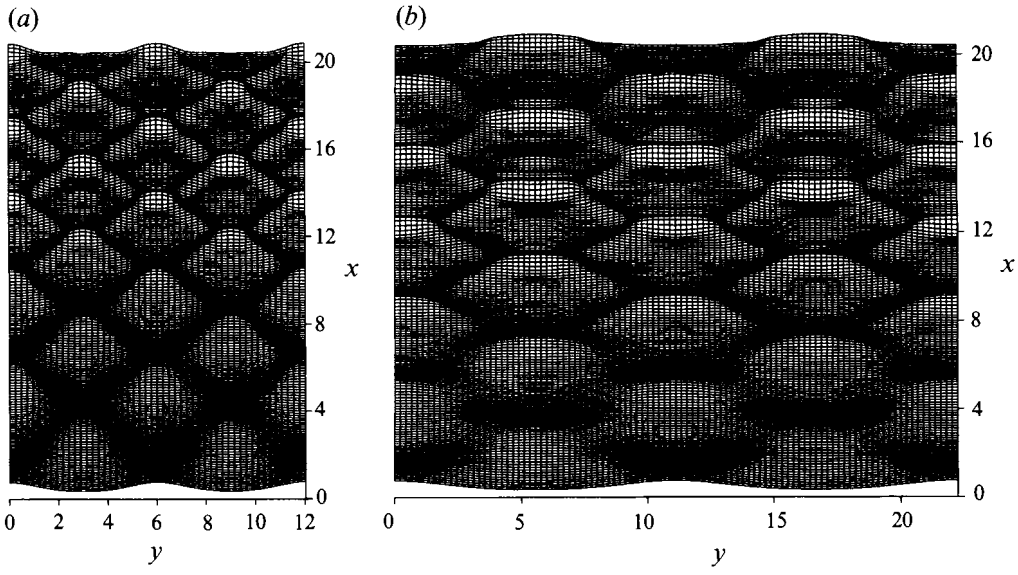

FIGURE 8. Three-dimensional plot of the free surface displacement for two cnoidal waves propagating over a slope with directed wave angles (*a*) $\theta_0 = \pm 45°$, (*b*) $\theta_0 = \pm 22.5°$ at time $t = nT (n = 0, 1, \ldots)$.

$h/\lambda_0 = 0$ to 0.5, where λ_0 represents the wavelength in deep water. The shoaling property of the equations has also been discussed. It turns out that the shoaling property imposes an additional restriction on the water depth limit allowable for the modified Boussinesq equations to be extended.

For regular waves propagating over a slowly varying topography, the governing equations for the velocity potentials of each harmonic are a set of weakly nonlinear coupled fourth-order elliptic equations with variable coefficients. The parabolic approximation has been applied to these fourth-order equations for the first time. We have found that the accuracy of the parabolic approximation to a fourth-order 'ordinary' differential equation with a weak forcing term (which may involve the other independent variable) depends on the difference between the wavenumber of the forcing term and the characteristic wavenumber of the equation. Both a small-angle parabolic model for waves propagating primarily in a dominant direction and an angular-spectrum parabolic model for multi-directional wave propagation have been derived and their validity has been tested. These models in principle can be extended to simulate irregular wave propagation by discretizing the power spectrum of the incident wave evenly (Freilich & Guza 1984; Madsen & Sørensen 1993). However, for a broad-banded spectrum, the implementation may be difficult and the parabolic models are not necessarily more efficient than direct simulation of the modified Boussinesq equations in the time domain. The angular-spectrum model is restricted to the situation where the deviation of the actual topography from a reference water depth (which varies in the on-offshore direction) is of the same order of magnitude as the typical wave amplitude and may not be applied to relatively deep water.

Although many examples have shown that the modified Boussinesq equations can be extended to relatively deep water, the velocity field calculated from (2.12) does not give accurate results. For regular waves, when the velocity field is essential, we

suggest an empirical formula to calculate the velocity potential $\Phi(x, y, z, t)$ once the velocity potential $\Phi_\alpha(x, y, t)$ is found:

$$\Phi(x, y, z, t) = \frac{\cosh k(z + h)}{\cosh k(z_\alpha + h)} \Phi_\alpha(x, y, t), \tag{6.1}$$

where k is given by (3.4). For an infinitesimal-amplitude periodic wave propagating in the x-direction over a constant depth, the maximum relative errors between the velocity components (u, w) given by above empirical formula and the exact velocity components (u_l, w_l) (without considering the nonlinearity) given by the linear theory over the range $h/\lambda_0 \in [0, 0.5]$ and $z/h \in [-1, 0]$ are

$$\max_{h/\lambda_0 \in [0,0.5], z/h \in [-1,0]} \{|u|/|u_l| - 1\} = 2.93\%, \tag{6.2}$$

$$\max_{h/\lambda_0 \in [0,0.5], z/h \in [-1,0]} \{|w|/|w_l| - 1\} = 2.94\%. \tag{6.3}$$

In relatively deep water, the nonlinearity should be very small to ensure the weak nonlinearity assumption is still valid in the shallow-water region. Therefore, as long as the bottom variation is small, the empirical formula (6.1) is a plausible way to find the velocity field in relatively deep water.

This research has been supported by a research grant from New York Sea Grant Institute and a research grant from the Army Research Office (DAAL 03-92-G-0116). We thank the reviewers for their comments and suggestions on the earlier version of this paper.

Appendix

This Appendix gives the dimensional forms of the small-angle model and angular-spectrum model. All variables shown in this Appendix are dimensional; however, primes have been dropped for simplicity.

In the dimensional form, the small-angle model, (4.42), becomes

$$\frac{\partial \Psi_n}{\partial x} = \mathrm{i}(k_n - k_n^*)\Psi_n + \frac{\mathrm{i}}{2k_n}\frac{\partial^2 \Psi_n}{\partial y^2} - \frac{1}{2k_n W_n}\left(P_n \frac{\partial k_n}{\partial x} + k_n R_n \frac{\partial h}{\partial x}\right)\Psi_n + \frac{\omega}{2(\alpha + 1/3)gh^3}\left(\sum_{s=1}^{n-1} \sigma_{ns}\Psi_s \Psi_{n-s} + \sum_{s=1}^{N-n} \gamma_{ns}\overline{\Psi}_s \Psi_{n+s}\right), \tag{A 1}$$

where

$$\beta_n(x, y) = h + \alpha n^2 \omega^2 h^2/g, \tag{A 2}$$

$$\tau_n(x, y) = 1 + z_\alpha n^2 \omega^2/g, \tag{A 3}$$

$$W_n(x, y) = \beta_n - 2(\alpha + 1/3)h^3 k_n^2, \tag{A 4}$$

$$R_n(x, y) = \tau_n - C_\alpha h^2 k_n^2, \tag{A 5}$$

$$P_n(x, y) = \beta_n - 6(\alpha + 1/3)h^3 k_n^2, \tag{A 6}$$

$$k_n^2(x, y) = \frac{\beta_n - \left[\beta_n^2 - 4(\alpha + 1/3)n^2\omega^2 h^3/g\right]^{1/2}}{2(\alpha + 1/3)h^3}, \tag{A 7}$$

$$(k_n^e)^2(x,y) = \frac{-\beta_n - \left[\beta_n^2 - 4(\alpha+1/3)n^2\omega^2h^3/g\right]^{1/2}}{2(\alpha+1/3)h^3}, \tag{A 8}$$

$$\sigma_{ns}(x,y) = \frac{\exp\left[\mathrm{i}(k_s^* + k_{n-s}^* - k_n^*)x\right] sk_{n-s}\left[\alpha h^2 k_s^2(k_s + k_{n-s}) - (2k_s + k_{n-s})\right]}{(k_{n-s} + k_s + k_n)\left[(k_{n-s}+k_s)^2 + (k_n^e)^2\right]}, \tag{A 9}$$

$$\begin{aligned}\gamma_{ns}(x,y) = \exp\left[\mathrm{i}(k_{n+s}^* - k_s^* - k_n^*)x\right] &\left[nk_sk_{n+s}(2+\alpha h^2k_sk_{n+s})\right.\\ &\left. + sk_{n+s}(k_{n+s} + \alpha h^2k_s^3) - (n+s)k_s(k_s + \alpha h^2k_{n+s}^3)\right]\\ &\times\left\{(k_{n+s} - k_s + k_n)\left[(k_{n+s}-k_s)^2 + (k_n^e)^2\right]\right\}^{-1}.\end{aligned} \tag{A 10}$$

The corresponding dimensional expression for the free surface displacement (4.4) is given by

$$\begin{aligned}g\zeta_n = \mathrm{i}n\omega\phi_n + \mathrm{i}n\omega&\left[\alpha h^2\left(\frac{\partial^2\phi_n}{\partial x^2} + \frac{\partial^2\phi_n}{\partial y^2}\right) + z_\alpha\frac{\partial h}{\partial x}\frac{\partial\phi_n}{\partial x}\right]\\ &- \frac{1}{4}\left[\sum_{s=1}^{n-1}\frac{\partial\phi_s}{\partial x}\frac{\partial\phi_{n-s}}{\partial x} + 2\sum_{s=1}^{N-n}\frac{\partial\bar{\phi}_s}{\partial x}\frac{\partial\phi_{n+s}}{\partial x}\right].\end{aligned} \tag{A 11}$$

The dimensional form of the angular-spectrum model, (4.76), is

$$\begin{aligned}\frac{\mathrm{d}\eta_n^l}{\mathrm{d}x} = &\left[\mathrm{i}(K_n^2 - t_l^2)^{1/2} - \frac{1}{4(K_n^2 - t_l^2)}\frac{E_{nl}}{F_n}\frac{\mathrm{d}K_n^2}{\mathrm{d}x}\right]\eta_n^l\\ &+ \frac{\mathrm{i}}{2F_n(K_n^2 - t_l^2)^{1/2}}\sum_{m=0}^{2M-1}Q_{ml}\left[U_n^m + \frac{\mathrm{i}\omega}{2g}V_n^m\right],\end{aligned} \tag{A 12}$$

where

$$B_n(x) = D + \alpha n^2\omega^2D^2/g, \tag{A 13}$$

$$K_n^2(x) = \frac{B_n - \left[B_n^2 - 4(\alpha+1/3)n^2\omega^2h^3/g\right]^{1/2}}{2(\alpha+1/3)h^3}, \tag{A 14}$$

$$F_n(x) = B_n - 2(\alpha+1/3)D^3K_n^2, \tag{A 15}$$

$$E_{nl}(x) = B_n - 2(\alpha+1/3)D^3(3K_n^2 - 2t_l^2), \tag{A 16}$$

$$\begin{aligned}U_n^m = (\beta_n^m - B_n)&\left[\frac{\mathrm{d}^2\phi_n^m}{\mathrm{d}x^2} + \frac{\partial^2\phi_n^m}{\partial y^2}\right] + (\alpha+1/3)\left[(h^m)^3 - D^3\right]\left[\frac{\mathrm{d}^4\phi_n^m}{\mathrm{d}x^4}\right.\\ &\left. + 2\frac{\partial^4\phi_n^m}{\partial x^2\partial y^2} + \frac{\partial^4\phi_n^m}{\partial y^4}\right] + \tau_n^m\left[\frac{\mathrm{d}h^m}{\mathrm{d}x}\frac{\mathrm{d}\phi_n^m}{\mathrm{d}x} + \frac{\partial h^m}{\partial y}\frac{\partial\phi_n^m}{\partial y}\right]\\ &+ (h^m)^2C_\alpha\left[\frac{\mathrm{d}h^m}{\mathrm{d}x}\left(\frac{\mathrm{d}^3\phi_n^m}{\mathrm{d}x^3} + \frac{\partial^3\phi_n^m}{\partial x\partial y^2}\right) + \frac{\partial h^m}{\partial y}\left(\frac{\partial^3\phi_n^m}{\partial x^2\partial y} + \frac{\partial^3\phi_n^m}{\partial y^3}\right)\right],\end{aligned} \tag{A 17}$$

$$\begin{aligned}V_n^m = \sum_{s=1}^{n-1}s\left\{2\left[\frac{\mathrm{d}\phi_s^m}{\mathrm{d}x}\frac{\mathrm{d}\phi_{n-s}^m}{\mathrm{d}x} + \frac{\partial\phi_s^m}{\partial y}\frac{\partial\phi_{n-s}^m}{\partial y}\right] + \alpha(h^m)^2\left[\left(\frac{\mathrm{d}^3\phi_s^m}{\mathrm{d}x^3} + \frac{\partial^3\phi_s^m}{\partial x\partial y^2}\right)\right.\right.\\ \left.\times\frac{\mathrm{d}\phi_{n-s}^m}{\mathrm{d}x} + \left(\frac{\partial^3\phi_s^m}{\partial x^2\partial y} + \frac{\partial^3\phi_s^m}{\partial y^3}\right)\frac{\partial\phi_{n-s}^m}{\partial y}\right] + \left[\phi_s^m + \alpha(h^m)^2\right.\end{aligned}$$

$$\times \left(\frac{\mathrm{d}^2\phi_s^m}{\mathrm{d}x^2}+\frac{\partial^2\phi_s^m}{\partial y^2}\right)\Bigg]\left[\frac{\mathrm{d}^2\phi_{n-s}^m}{\mathrm{d}x^2}+\frac{\partial^2\phi_{n-s}^m}{\partial y^2}\right]\Bigg\}+\sum_{s=1}^{N-n}\Bigg\{n\Bigg[2\left(\frac{\mathrm{d}\bar{\phi}_s^m}{\mathrm{d}x}\frac{\mathrm{d}\phi_{n+s}^m}{\mathrm{d}x}+\frac{\partial\bar{\phi}_s^m}{\partial y}\frac{\partial\phi_{n+s}^m}{\partial y}\right)+\alpha(h^m)^2\left(\frac{\mathrm{d}^2\bar{\phi}_s^m}{\mathrm{d}x^2}+\frac{\partial^2\bar{\phi}_s^m}{\partial y^2}\right)\left(\frac{\mathrm{d}^2\phi_{n+s}^m}{\mathrm{d}x^2}+\frac{\partial^2\phi_{n+s}^m}{\partial y^2}\right)\Bigg]$$
$$-s\Bigg[\alpha(h^m)^2\left(\left(\frac{\mathrm{d}^3\bar{\phi}_s^m}{\mathrm{d}x^3}+\frac{\partial^3\bar{\phi}_s^m}{\partial x\partial y^2}\right)\frac{\mathrm{d}\phi_{n+s}^m}{\mathrm{d}x}+\left(\frac{\partial^3\bar{\phi}_s^m}{\partial x^2\partial y}+\frac{\partial^3\bar{\phi}_s^m}{\partial y^3}\right)\frac{\partial\phi_{n+s}^m}{\partial y}\right)$$
$$+\bar{\phi}_s^m\left(\frac{\mathrm{d}^2\phi_{n+s}^m}{\mathrm{d}x^2}+\frac{\partial^2\phi_{n+s}^m}{\partial y^2}\right)\Bigg]+(n+s)\Bigg[\alpha(h^m)^2\left(\left(\frac{\mathrm{d}^3\phi_{n+s}^m}{\mathrm{d}x^3}+\frac{\partial^3\phi_{n+s}^m}{\partial x\partial y^2}\right)\frac{\mathrm{d}\bar{\phi}_s^m}{\mathrm{d}x}$$
$$+\left(\frac{\partial^3\phi_{n+s}^m}{\partial x^2\partial y}+\frac{\partial^3\phi_{n+s}^m}{\partial y^3}\right)\frac{\partial\bar{\phi}_s^m}{\partial y}\right)+\phi_{n+s}^m\left(\frac{\mathrm{d}^2\bar{\phi}_s^m}{\mathrm{d}x^2}+\frac{\partial^2\bar{\phi}_s^m}{\partial y^2}\right)\Bigg]\Bigg\}. \tag{A 18}$$

The derivatives appearing in (A 17) and (A 18) are given by

$$\frac{\partial h^m}{\partial y}=\Lambda_0^{1/2}\sum_{j=0}^{2M-1}[D_1]_{mj}h^j,\qquad \frac{\partial^3\phi_s^m}{\partial x^2\partial y}=\Lambda_0^{1/2}\sum_{j=0}^{2M-1}[D_1]_{mj}\frac{\mathrm{d}^2\phi_s^j}{\mathrm{d}x^2}, \tag{A 19}$$

$$\frac{\partial^3\phi_s^m}{\partial x\partial y^2}=\Lambda_0\sum_{j=0}^{2M-1}[D_2]_{mj}\frac{\mathrm{d}\phi_s^j}{\mathrm{d}x},\qquad \frac{\partial^4\phi_s^m}{\partial x^2\partial y^2}=\Lambda_0\sum_{j=0}^{2M-1}[D_2]_{mj}\frac{\mathrm{d}^2\phi_s^j}{\mathrm{d}x^2}, \tag{A 20}$$

where

$$\frac{\mathrm{d}^p\phi_s^m}{\mathrm{d}x^p}=\sum_{q=0}^{2M-1}\mathrm{i}^p(K_n^2-t_q^2)^{p/2}Q_{mq}\eta_s^q, \tag{A 21}$$

$$\frac{\partial^p\phi_s^m}{\partial y^p}=\Lambda_0^{p/2}\frac{\partial^p\phi_s(x,\tilde{y}_m)}{\partial\tilde{y}^p}=\Lambda_0^{p/2}\sum_{j=0}^{2M-1}[D_p]_{mj}\phi_s^j, \tag{A 22}$$

$$\phi_s^j=\sum_{q=0}^{2M-1}Q_{jq}\eta_s^q. \tag{A 23}$$

REFERENCES

Akylas, T. R. 1994 Three-dimensional long water-wave phenomena. *Ann. Rev. Fluid Mech.* **26**, 191–210.

Chen, Y. 1995 Modelling of surface water wave and interfacial wave propagation. Doctoral dissertation, Cornell University, Ithaca, New York.

Chen, Y. & Liu, P. L.-F. 1994 A pseudospectral approach for scattering of water waves. *Proc. R. Soc. Lond.* A **445**, 619–636.

Chen, Y. & Liu, P. L.-F. 1995 The unified Kadomtsev–Petviashvili equation for interfacial waves. *J. Fluid Mech.* **288**, 383–408.

Freilich, M. H. & Guza, R. T. 1984 Nonlinear effects on shoaling surface gravity waves. *Phil. Trans. R. Soc. Lond.* A **311**, 1–41.

Gottlieb, D., Hussaini, M. Y. & Orszag, S. A. 1984 Introduction: Theory and applications of spectral methods. In *Spectral Methods for Partial Differential Equations* (ed. R. G. Voigt, D. Gottlieb & M. Y. Hussaini), pp. 1–54. SIAM, Philadelphia.

Hammack, J., Scheffner, N. & Segur, H. 1988 Two-dimensional periodic waves in shallow water. *J. Fluid Mech.* **209**, 567–589.

Kirby, J. T. 1990 Modelling shoaling directional wave spectra in shallow water. In *Proc. 22nd Int. Conf. on Coastal Engineering, Delft, The Netherlands*, pp. 109–122.

KIRBY, J. T. 1991 Intercomparison of truncated series solutions for shallow water waves. *J. Waterway, Port, Coastal, Ocean Engng, ASCE* **117**, 143–155.

LIU, P. L.-F. & TSAY, T. K. 1984 Refraction-diffraction model for weakly nonlinear water waves. *J. Fluid Mech.* **141**, 265–274.

LIU, P. L.-F., YOON, S. B. & KIRBY, J. T. 1985 Nonlinear refraction-diffraction of waves in shallow water. *J. Fluid Mech.* **153**, 185–201.

MADSEN, P. A., MURRAY, R. & SØRENSEN, O. R. 1991 A new form of the Boussinesq equations with improved linear dispersion characteristics. *Coastal Engng* **15**, 371–388.

MADSEN, P. A. & SØRENSEN, O. R. 1992 A new form of the Boussinesq equations with improved linear dispersion characteristics. Part 2. A slowly-varying bathymetry. *Coastal Engng* **18**, 183–204.

MADSEN, P. A. & SØRENSEN, O. R. 1993 Bound waves and triad interactions in shallow water. *Ocean Engng* **20**, 359–388.

MCCOWAN, A. D. & BLACKMAN, D. R. 1989 The extension of Boussinesq type equations to modelling short waves in deep water. In *Proc. 9th Australasian Conference on Coastal and Ocean Engineering, Adelaide Australia*, pp. 412–416.

NWOGU, O. 1993*a* Alternative form of Boussinesq equations for nearshore wave propagation. *J. Waterway, Port, Coastal, Ocean Engng, ASCE* **119**, 618–638.

NWOGU, O. 1993*b* Nonlinear transformation of multi-directional waves in water of variable depth. (Submitted for publication)

PEREGRINE, D. H. 1967 Long waves on a beach. *J. Fluid Mech.* **27**, 815–827.

RYGG, O. 1988 Nonlinear refraction-diffraction of surface waves in intermediate and shallow water. *Coastal Engng* **12**, 191–211.

RADDER, A. C. 1979 On the parabolic equation method for water-wave propagation. *J. Fluid Mech.* **95**, 159–176.

SKOVGAARD, O. & PETERSEN, M. H. 1977 Refraction of cnoidal waves. *Coastal Engng* **1**, 43–61.

WHALIN, R. W. 1971 The limit of applicability of linear wave refraction theory in a convergence zone. *Res. Rep.* H-71-3. U.S. Army Corps of Engrs, Waterways Expt. Station, Vicksburg, MS.

WITTING, J. M. 1984 A unified model for the evolution of nonlinear water waves. *J. Comput. Phys.* **56**, 203–236.

WU, T. Y. 1979 On tsunamis propagation – evaluation of existing models. In *Tsunamis – Proceedings of the National Science Foundation Workshop* (ed. L. S. Hwang & Y. K. Lee), pp. 110–149. Pasadena, CA: Tetra Tech. Inc.

YOON, S. B. & LIU, P. L.-F. 1989 Stem waves along breakwater. *J. Waterway, Port, Coastal, Ocean Engng, ASCE* **115**, 635–648.